1  **Brain stimulation boosts perceptual learning by altering sensory GABAergic plasticity**

2  **and functional connectivity**

3  Vasilis M Karlaftis*[1], Polytimi Frangou*[1], Cameron Higgins[2], Diego Vidaurre[2,3], Joseph J

4  Ziminski[1], Charlotte J Stagg[2], Uzay E Emir[4], Zoe Kourtzi[1]

5

6  [1]Department of Psychology, University of Cambridge, Cambridge UK

7  [2]Wellcome Centre for Integrative Neuroimaging, University of Oxford, Oxford, UK

8  [3]Center of Functionally Integrative Neuroscience, Department of Clinical Medicine, Aarhus

9  University, Aarhus, Denmark

10  [4]Purdue University School of Health Sciences, West Lafayette, Indiana, USA

11  *These authors contributed equally to this work

12

13  *Short title*: tDCS-induced learning and brain plasticity

14

15  *Corresponding author:*

16  Zoe Kourtzi

17  Department of Psychology

18  University of Cambridge

19  Downing Street, CB2 3EB

20  Cambridge, UK

21  Email: zk240@cam.ac.uk

22    **Abbreviations**

23    CRLB: Cramer-Rao lower bound

24    CSF: cerebrospinal fluid

25    EPI: echo-planar imaging

26    FO: Fractional Occupancy

27    Glu: Glutamate

28    HMM: Hidden Markov Models

29    ICA: Independent Component Analysis

30    IPS: intra-parietal sulcus

31    MNI: Montreal Neurological Institute

32    MRS: Magnetic Resonance Spectroscopy

33    NAA: N acetylaspartate

34    OCT: occipito-temporal cortex

35    PCA: Principal Component Analysis

36    ROI: region of interest

37    rs-fMRI: resting-state functional Magnetic Resonance Imaging

38    SN: signal-in-noise

39    SNR: Signal-to-noise ratio

40    SR: Switching Rate

41    tDCS: transcranial direct current stimulation

## Abstract

Interpreting cluttered scenes —a key skill for successfully interacting with our environment— relies on our ability to select relevant sensory signals while filtering out noise. Training is known to improve our ability to make these perceptual judgements by altering local processing in sensory brain areas. Yet, the brain-wide network mechanisms that mediate our ability for perceptual learning remain largely unknown. Here, we combine transcranial direct current stimulation (tDCS) with multi-modal brain measures to modulate cortical excitability during training on a signal-in-noise task (i.e. detection of visual patterns in noise) and test directly the link between processing in visual cortex and its interactions with decision-related areas (i.e. posterior parietal cortex). We test whether brain stimulation alters inhibitory processing in visual cortex, as measured by magnetic resonance spectroscopy (MRS) of GABA and functional connectivity between visual and posterior parietal cortex, as measured by resting state functional magnetic resonance imaging (rs-fMRI). We show that anodal tDCS during training results in faster learning and decreased GABA+ during training, before these changes occur for training without stimulation (i.e. sham). Further, anodal tDCS decreases occipito-parietal interactions and time-varying connectivity across the visual cortex. Our findings demonstrate that tDCS boosts learning by accelerating visual GABAergic plasticity and altering interactions between visual and decision-related areas, suggesting that training optimises gain control mechanisms (i.e. GABAergic inhibition) and functional inter-areal interactions to support perceptual learning.

62    **Introduction**

63    Interacting successfully in our environments entails discerning relevant information from

64    clutter and identifying target objects in busy scenes. Training is shown to improve such

65    perceptual judgements —a skill known as perceptual learning— by altering processing in

66    sensory (i.e. visual) and decision-related (i.e. posterior parietal) areas. For example, perceptual

67    learning (i.e. training on a visual discrimination task) has been shown to alter functional

68    connectivity —as measured by rs-fMRI— between visual and posterior parietal cortex (Lewis

69    et al., 2009). Further, we have previously shown that training in visual discrimination tasks

70    alters GABAergic processing in visual cortex (Frangou et al., 2019, 2018) —as measured by

71    MRS—, consistent with the role of GABAergic inhibition in brain plasticity (for a review see

72    (Ip and Bridge, 2021)). Yet, the interactions between GABAergic plasticity in sensory areas

73    and learning-dependent functional connectivity between sensory and decision-related areas for

74    perceptual learning remain largely unknown.

75           Previous work has proposed that GABAergic inhibition shapes network connectivity

76    (Kapogiannis et al., 2013; Mann and Paulsen, 2007; Shmuel and Leopold, 2008; Stagg et al.,

77    2014). Here, we employ tDCS to modulate cortical excitability and test directly the link

78    between local inhibitory processing in visual cortex —as measured by MRS GABA— and

79    interactions between visual and decision-related areas (i.e. posterior parietal cortex) —as

80    measured by static and time-varying (using Hidden Markov Models (HMM; (Vidaurre et al.,

81    2018, 2017)) rs-fMRI connectivity. Anodal tDCS has been shown to be excitatory (Antal et al.,

82    2004a; Nitsche and Paulus, 2000), result in decreased GABA levels in visual (Barron et al.,

83    2016), frontal (Harris et al., 2019) and motor areas (Stagg et al., 2009), and facilitate visual

84    (Frangou et al., 2018; Sczesny-Kaiser et al., 2016; Van Meel et al., 2016) and motor learning

85    (O'Shea et al., 2017; Stagg et al., 2011). Further, anodal tDCS in the motor cortex has been

86  shown to facilitate learning by decreasing local GABA levels and increasing functional

87  connectivity within the motor network at rest (Bachtiar et al., 2015; Stagg et al., 2014).

88      We ask whether anodal tDCS in occipito-temporal cortex (OCT) facilitates learning

89  and alters GABAergic processing and brain network interactions. We trained participants in a

90  signal-in-noise discrimination task (i.e. participants were asked to detect radial vs. concentric

91  patterns embedded in noise) that has been shown to involve occipito-temporal and posterior

92  parietal cortex (Chang et al., 2014; Frangou et al., 2019, 2018; Mayhew et al., 2012). We tested

93  for changes in task performance, MRS GABA+ and rs-fMRI connectivity in three groups of

94  participants: two intervention groups who received anodal vs. sham tDCS during training on

95  the task, a no-intervention group who received neither stimulation nor training in the task. Our

96  results show that anodal OCT stimulation results in faster learning and decreased GABA+

97  during training, before these changes occur in the sham stimulation group. Further, anodal

98  tDCS induces changes in occipito-parietal interactions and time-varying connectivity across

99  the visual cortex. Finally, enhanced local temporal coherence in the visual cortex and decreased

100  occipito-parietal connectivity relate to decreased OCT GABA+. Our findings suggest that

101  tDCS boosts learning by altering visual GABAergic processing and network interactions

102  between visual and decision-related areas.

5

**Results**

**Anodal tDCS improves performance in signal-in-noise discrimination**

We trained two intervention groups (anodal vs. sham tDCS on OCT) on a signal-in-noise (SN) task that involves participants discriminating shapes (radial vs. concentric Glass patterns) embedded in noise (Figure 1). Participants were asked to judge whether each stimulus presented per trial was radial vs. concentric.

Figure 1

We tested behavioural improvement in this task by comparing performance before (Pre), during (During) and after stimulation (Post) (see *Behavioural data analysis* in Methods). Our results showed that anodal OCT stimulation enhanced behavioural improvement in this task (Figure 2a), consistent with our previous work (Frangou et al., 2018). In particular, a two-way repeated measures ANOVA showed a significant Group (Anodal, Sham) x Block (Pre, During, Post) interaction ($F(1.78,76.40)=3.61$, $p=0.037$) and main effect of Block ($F(1.78,76.40)=8.94$, $p<0.001$). Performance before stimulation (i.e. Pre block) did not differ significantly between the two intervention groups ($t(43)=1.02$, $p=0.313$), suggesting that the observed differences in improvement were not due to variability in starting performance between the intervention groups. Further, comparing learning rate across training between the two groups (two-sample t-test) showed that participants in the Anodal group learned faster than participants in the Sham group ($t(43)=2.31$, $p=0.026$; Figure 2b).

Participants in the no-intervention (Control) group (i.e. no-stimulation, no-training group) showed no behavioural improvement in the SN task when we tested them before and after the scan ($t(20)=0.18$, $p=0.858$) nor in the contrast-detection task during the scan (one-way repeated measures ANOVA: main effect of Block: $F(2.19,46.03)=0.82$, $p=0.458$).

Figure 2

**Anodal tDCS results in GABA+ decrease earlier in training**

To test whether anodal tDCS alters GABAergic inhibition in OCT, we measured GABA+ within an MRS voxel centred in the OCT (Figure 3) before, during and after anodal vs. sham stimulation in the OCT, while participants trained on the SN task. We compared GABA+ in the OCT for the intervention groups (i.e. anodal and sham stimulation groups who received task training) vs. the no-intervention group (i.e. no-stimulation, no-training). Comparing GABA+ change between groups, a two-way repeated measures ANOVA showed a significant Group (Anodal, Sham, Control) x Block (Pre, During, Post) interaction ($F(4,120)=3.90$, $p=0.005$; Figure 4a) and main effect of Group ($F(2,60)=5.25$, $p=0.008$). Post-hoc comparisons across blocks showed significantly decreased GABA+ for the Anodal compared to the Control group ($t=-3.21$, $p=0.006$, Bonferroni corrected), but no significant difference between Sham and Control ($t=-1.93$, $p=0.174$, Bonferroni corrected) or Anodal and Sham ($t=-1.22$, $p=0.678$, Bonferroni corrected). Further, comparing the Anodal to the Control group showed significantly decreased GABA+ for both During ($t(41)=-2.23$, $p=0.031$) and Post blocks ($t(41)=-3.77$, $p=0.001$). In contrast, comparing the Sham to the Control group showed significantly decreased GABA+ for the Post ($t(40)=-2.66$, $p=0.011$) but not the During block ($t(40)=-0.88$, $p=0.387$). These results remained significant when we tested GABA+ referenced to N acetylaspartate (NAA) rather than water (Group x Block: $F(4,120)=4.06$, $p=0.004$; main effect of Group: $F(2,60)=6.35$, $p=0.003$; Anodal vs. Control: $t=-3.53$, $p=0.002$, Bonferroni corrected; Anodal vs. Control at During block: $t(41)=-2.74$, $p=0.009$, Anodal vs. Control at Post block: $t(41)=-4.46$, $p<0.001$; Sham vs. Control at Post block: $t(40)=-2.78$, $p=0.008$). Thus, our results demonstrate that training with (anodal) or without stimulation (sham) results in decreased GABA+ in visual cortex compared to a no intervention (i.e. no training nor stimulation) control. Interestingly, training with anodal stimulation decreases GABA+ in the OCT during and after stimulation, compared to training without stimulation (i.e. sham) that

153    shows decreases in GABA+ only after stimulation. These results suggest that anodal

154    stimulation induces neurochemical changes earlier in the training, consistent with our

155    behavioural results showing faster learning for anodal stimulation.

156                                                    Figure 3

157

158    It is unlikely that these changes in GABA+ for the intervention groups were due to differences

159    in MRS data quality (i.e. linewidth, Signal-to-noise ratio: SNR) between groups (Table S1). In

160    particular, a two-way repeated measures ANOVA showed no significant Group x Block

161    interaction (linewidth: $F_{(4,120)}=0.32$, p=0.864; SNR: $F_{(4,120)}=0.72$, p=0.581) nor main effect

162    of Group (linewidth: $F_{(2,60)}=1.44$, p=0.246; SNR: $F_{(2,60)}=0.85$, p=0.432). Further, GABA+

163    measured before stimulation did not significantly differ between groups (main effect of Group:

164    $F_{(2,60)}=2.20$, p=0.120), suggesting that our results could not be simply due to variability in

165    GABA+ before stimulation across groups. Finally, comparing glutamate measures between

166    groups showed no significant Group x Block interaction ($F_{(4,120)}=0.80$, p=0.528) nor main

167    effect of Group ($F_{(2,60)}=0.37$, p=0.692) or Block ($F_{(2,120)}=1.33$, p=0.269), suggesting that

168    our results are specific to GABA+.

169           Next, we tested whether changes in OCT GABA+ relate to behavioural performance.

170    We computed percent GABA+ change during tDCS (During) compared to GABA+ before

171    stimulation (Pre) to control for variability in baseline GABA+ measures (i.e. Pre). We

172    measured GABA+ change during stimulation as our previous analysis showed GABA+

173    changes during stimulation for the Anodal rather than the Sham group (Figure 4a). Correlating

174    OCT GABA+ change with learning rate showed a significant negative correlation for the

175    Anodal group ($r(19)=-0.51$, p=0.019; Figure 4b), but not for the Sham group ($r(18)=0.25$,

176    p=0.289; Figure 4b). These correlations were significantly different between groups (Fisher's

177    z test: z=-2.41, p=0.016). Further, this relationship remained significant when controlling for

178  tissue composition within the MRS voxel, controlling for MRS data quality (i.e. linewidth,

179  SNR), and using GABA+ referenced to NAA rather than water (Table S2). There was no

180  significant correlation for OCT Glutamate (Glu) change and learning rate, suggesting that this

181  result is specific to GABA (Table S2). We found no significant correlation between learning

182  rate on the contrast-detection task and change in GABA+ for the Control group (r(20)=0.06,

183  p=0.790). Finally, there was no significant correlation between learning rate and OCT GABA+

184  change for the post- compared to the pre-stimulation block for any group (Anodal: r(18)=-0.19,

185  p=0.417; Sham: r(18)=0.17, p=0.473; Control: r(20)=0.02, p=0.945), suggesting that our

186  results are specific to the GABA+ change during stimulation. These results demonstrate that

187  learning-dependent changes in GABA+ during training with anodal stimulation rather than

188  training without stimulation (i.e. sham) relate to learning rate, suggesting that enhanced

189  GABAergic plasticity due to tDCS in the OCT may facilitate faster learning in detecting targets

190  in clutter.

191                                    Figure 4

192

193  **Anodal tDCS alters functional connectivity**

194  We next tested whether anodal tDCS during training on the SN task alters extrinsic (i.e.

195  between OCT and intra-parietal sulcus [IPS]) or intrinsic (i.e. within OCT) connectivity as

196  measured by rs-fMRI. First, we tested for changes in extrinsic OCT-IPS connectivity after vs.

197  before intervention. A two-way repeated measures ANOVA showed a significant Group

198  (Anodal, Sham) x Block (Pre, Post) interaction (F(1,35)=7.96, p=0.008; Figure 5a), but no

199  significant main effect of Group (F(1,35)=2.44, p=0.127) or Block (F(1,35)=0.01, p=0.924).

200  Post-hoc comparisons showed a significant decrease in OCT-IPS connectivity after training for

201  the Anodal group (t(21)=-2.16, p=0.042), but no significant change for the Sham group

202  (t(14)=1.96, p=0.071). Next, we asked whether changes in extrinsic connectivity relate to

203    behaviour (i.e. learning rate) and OCT GABA+ change during stimulation, as our analysis

204    showed GABA+ changes during stimulation that relate to behaviour for the Anodal rather than

205    the Sham group. We found a significant positive correlation of OCT-IPS connectivity change

206    with learning rate for the Sham (r(11)=0.74, p=0.003; Figure 5b), but not for the Anodal group

207    (r(20)=-0.24, p=0.286; Figure 5b). Comparing these correlations showed a significant

208    difference between groups (Fisher's z test: z=-3.06, p=0.002). Further, we found a significant

209    positive correlation of change in OCT-IPS connectivity with change in OCT GABA+ for the

210    Anodal (r(17)=0.48, p=0.036; Figure 5c), but not for the Sham group (r(13)=0.13, p=0.643;

211    Figure 5c). This relationship remained significant when controlling for tissue composition

212    within the MRS voxel, controlling for MRS data quality, and using GABA+ referenced to NAA

213    rather than water (Table S3). There was no significant correlation for OCT Glu change and

214    learning rate, suggesting that this result is specific to GABA (Table S3).

215        These results demonstrate that anodal OCT stimulation results in decreased occipito-

216    parietal connectivity after training that relates to decreased OCT GABA+ during stimulation,

217    suggesting that enhanced GABAergic plasticity due to tDCS in the OCT may relate to local

218    visual processing rather than occipito-parietal interactions. In contrast, for task training without

219    stimulation (i.e. sham stimulation), learning-dependent changes in occipito-parietal

220    connectivity relate to faster learning but not changes in GABA+.

221                                          Figure 5

222

223        Second, we tested for changes in intrinsic OCT connectivity after vs. before

224    intervention. A two-way repeated measures ANOVA showed a significant main effect of Block

225    (Pre, Post) (F(1,35)=4.66, p=0.038; Figure 6a), but no significant Group (Anodal, Sham) x

226    Block (Pre, Post) interaction (F(1,35)=0.55, p=0.463), nor main effect of Group (F(1,35)=3.13,

227    p=0.086). Next, we asked whether changes in intrinsic connectivity relates to learning rate and

228    OCT GABA+ change (during- vs. pre-stimulation). There were no significant correlations of

229    change in intrinsic OCT connectivity with learning rate (Anodal: r(20)=0.26, p=0.249; Sham:

230    r(12)=0.52, p=0.056; Figure 6b). However, we observed a significant negative correlation for

231    change in intrinsic OCT connectivity with change in OCT GABA+ for the Anodal group

232    (r(14)=-0.52, p=0.039; Figure 6c), but not for the Sham group (r(13)=0.21, p=0.453; Figure

233    6c). This relationship remained significant when controlling for tissue composition within the

234    MRS voxel, controlling for MRS data quality, and using GABA+ referenced to NAA rather

235    than water (Table S3). There was no significant correlation for OCT Glu change and learning

236    rate, suggesting that this result is specific to GABA (Table S3). Taken together, our results

237    show that increased local OCT connectivity relates to decreases in OCT GABA+ during anodal

238    but not sham stimulation, providing converging evidence that enhanced GABAergic plasticity

239    due to anodal tDCS in the OCT relates to local visual processing.

240                                                    Figure 6

241

242    **Anodal tDCS alters time-varying functional connectivity during training**

243    Our functional connectivity analysis shows that our intervention (anodal tDCS during task

244    training) alters occipito-parietal interactions that relate to GABAergic plasticity. However,

245    static connectivity offers a summary measure of the synchrony between two brain regions

246    across long timescales (i.e. 8mins for our rs-fMRI scans) that does not capture short-lived

247    changes in inter-regional synchrony and how they propagate across different brain regions.

248    Recent studies have proposed time-varying connectivity approaches for tracking changes in

249    functional connectivity at finer timescales (Cohen, 2017; Hutchison et al., 2013; Preti et al.,

250    2017). These methods have been shown to capture task and behavioural variability beyond

251    static connectivity accounts (Calhoun et al., 2014; Eichenbaum et al., 2021). Here, we employ

252    a time-varying connectivity analysis (i.e. HMM) to detect brain states that capture recurring

11

253    patterns of activity and connectivity over time and test whether our intervention alters these

254    brain states.

255        We conducted this analysis using time courses from early and higher visual areas and

256    posterior parietal cortex as defined by a topographic atlas ((Wang et al., 2015); Table S4). We

257    set the number of states to 5 and decomposed the input time courses to 13 Principal Component

258    Analysis (PCA) components (corresponding to 80% variance explained) across groups and

259    blocks. Following previous work (Karapanagiotidis et al., 2020; Vidaurre et al., 2017), we then

260    tested the robustness of the results for a range of these parameters (states: from 4 to 7, PCA:

261    from 70% to 100%; Table S5). The 5 estimated states capture reoccurring temporal patterns

262    across participants and are described by a mean activation map (Figure 7a) and a functional

263    connectivity matrix (Figure S1): State 1 captures concurrent deactivation across all regions;

264    State 2 captures time periods when OCT (i.e. LO1/2), IPS (i.e. IPS0 and IPS1/2) and V3b are

265    co-active; State 3 captures time periods when V1 (dorsal and ventral) V2 (dorsal) are co-active;

266    State 4 captures concurrent activation across all regions; State 5 captures time periods when

267    IPS (i.e. IPS0), PHC, V3a and VO are co-active. Figure 7b illustrates the transition probabilities

268    between these states averaged across participants, where higher (lower) values represent more

269    (less) likely transitions from one state to another.

270                                    Figure 7

271

272        To test for temporal differences between anodal and sham OCT stimulation, we

273    compared the time spent in each state (i.e. Fractional Occupancy: FO) before vs. after training

274    per group. A two-way repeated measures ANOVA showed a significant State x Block

275    interaction for the Anodal group ($F(1.45,27.93)=6.22$, $p=0.010$; Figure 7c), but no significant

276    effects for the Sham group ($F(1.35,18.82)=1.14$, $p=0.319$; Figure 7c). Post-hoc comparisons

277    showed that participants in the Anodal group spent more time after training in States 1 and 4

12

278    (State 1: t(21)=2.21, p=0.038; State 4: t(21)=3.46, p=0.002); that is, they spent more time in

279    states capturing time periods of widespread concurrent deactivation and activation across the

280    visual cortex. Previous work has suggested that large-scale synchronised activity might denote

281    integration of information (Varela et al., 2001) and higher sensitivity in error detection

282    (Breakspear et al., 2003). In contrast, participants in the Anodal group spent less time in States

283    2 and 3 (State 2: t(21)=-2.44, p=0.023; State 3: t(21)=-2.63, p=0.015) that correspond to the

284    OCT-IPS and the early visual (V1, V2) states, respectively. Comparing the switching rate (SR)

285    between states before vs. after training showed that participants in the Anodal group switched

286    more frequently between states after training (t(21)=2.30, p=0.032), while there was no

287    significant change for the Sham group (t(14)=1.19, p=0.254).

288        These results complement our static connectivity results showing that anodal OCT

289    stimulation during training in the SN task results in more widespread visual activity, and less

290    localised activity in occipito-parietal and early visual regions. Further, anodal OCT stimulation

291    may facilitate faster processing within brain states, as indicated by faster switching rate

292    between states after training in the SN task.

**Discussion**

Previous work has shown that training results in changes in GABAergic inhibition that relate to improved performance in visual (Frangou et al., 2019, 2018; Shibata et al., 2017) and motor tasks (Kolasinski et al., 2019; Sampaio-Baptista et al., 2015). Here, we employ tDCS to modulate cortical excitability (Antal et al., 2004a; Nitsche and Paulus, 2000) and test the role of GABAergic inhibition in perceptual learning. tDCS has been shown to alter performance in visual tasks (Antal et al., 2004b; Battaglini et al., 2017; Spiegel et al., 2013; Zito et al., 2015) and facilitate learning in motor (O'Shea et al., 2017) and visual memory tasks (Barron et al., 2016) by reducing GABA. Here, we demonstrate that modulating GABAergic inhibition with tDCS during training boosts performance in perceptual judgements by altering local processing in visual cortex and functional connectivity between visual and posterior parietal areas that are involved in perceptual decision making. Our findings advance our understanding of GABAergic plasticity mechanisms for perceptual learning in the following respects.

First, we have previously shown that anodal tDCS during training enhances behavioural improvement on the signal-in-noise task that has been shown to relate to decreased GABAergic inhibition (Frangou et al., 2018). Here, we demonstrate that tDCS dissociates faster vs. slower learning and GABAergic plasticity. In particular, we show that training with anodal stimulation on the visual cortex results not only in behavioural improvement, but also faster learning compared to training without stimulation (i.e. sham stimulation). Further, training with anodal tDCS results in decreased OCT GABA+ during and after stimulation, in contrast to training without stimulation (i.e. sham) that shows a later decrease in OCT GABA+ (i.e. after stimulation). Next, we show that this decrease in GABA+ during anodal stimulation relates to faster learning, suggesting that anodal OCT stimulation during training accelerates perceptual learning by shifting GABAergic plasticity in the OCT earlier in the learning process.

14

317    Second, previous studies have shown that training in a range of tasks (e.g. motor or

318    perceptual tasks) results in changes in functional connectivity (Guerra-Carrillo et al., 2014;

319    Karlaftis et al., 2019; Kelly and Castellanos, 2014; Lewis et al., 2009; Sampaio-Baptista et al.,

320    2015). Further, functional connectivity has been shown to relate to GABAergic inhibition

321    (Frangou et al., 2019; Kapogiannis et al., 2013; Karlaftis et al., 2021; Mann and Paulsen, 2007;

322    Nasrallah et al., 2017; Sampaio-Baptista et al., 2015; Shmuel and Leopold, 2008; Stagg et al.,

323    2014) and can be altered by tDCS during training in a range of tasks: spatial navigation

324    (Krishnamurthy et al., 2015), associative learning (Krause et al., 2017), language processing

325    (Cao and Liu, 2018; Meinzer et al., 2012), visual selective attention (McDermott et al., 2019)

326    and visual search (Callan et al., 2016). In our previous work, we showed that perceptual

327    learning in the signal-in-noise task relates to functional connectivity within visual cortex and

328    between visual and posterior parietal regions measured at rest before training (Frangou et al.,

329    2019). Here, we test whether combining brain stimulation with training results in changes in

330    functional connectivity. Our results demonstrate that anodal —rather than sham— OCT

331    stimulation during training, decreases occipito-parietal connectivity. This is consistent with

332    previous work showing that IPS is involved in identifying salient and task-relevant features

333    early in training, while OCT is involved in tuning task-relevant feature representation after

334    training (Chang et al., 2014; Frangou et al., 2019; Mayhew et al., 2012). In particular, our

335    results show that increased occipito-parietal connectivity relates to faster learning for

336    participants in the Sham group, who show slower improvement and are therefore engaged in

337    earlier stages of learning. In contrast, for the Anodal group, occipito-parietal connectivity

338    shows a significant decrease that correlates with OCT GABA+ decrease during our

339    intervention (stimulation and training). The relationship between tDCS-induced changes in

340    GABAergic inhibition and functional connectivity remains debated, with some studies

341    showing a significant relationship (Antonenko et al., 2017), but some others not (e.g. (Bachtiar

15

342    et al., 2015)). Here, we show that anodal tDCS during training to detect targets in clutter results

343    in accelerated GABA decrease in visual cortex that relates to reduced occipito-parietal

344    connectivity, suggesting that anodal tDCS alters functional connectivity between sensory and

345    decision-related areas.

346         Further, we show a significant negative correlation between intrinsic connectivity

347    change and OCT GABA+ change during anodal but not sham stimulation (potentially due to

348    the delayed GABA decrease in the Sham group). This relationship between changes in OCT

349    GABA+ and local temporal coherence suggests that decreased GABAergic inhibition within

350    visual cortex may facilitate signal detection by enhancing local processing. This result is

351    consistent with our previous work showing higher intrinsic connectivity before training for

352    greater GABA decrease during training (Frangou et al., 2019).

353         Previous work has shown that time-varying connectivity captures task and behavioural

354    variability in addition to what is explained by static connectivity (Calhoun et al., 2014; Liégeois

355    et al., 2019; Vidaurre et al., 2021). Here, we employ HMM to detect brain states of recurrent

356    activity and connectivity patterns that have been linked to cognition (Karapanagiotidis et al.,

357    2020; Vidaurre et al., 2017) and investigate learning-dependent plasticity at a finer timescale.

358    We show that anodal stimulation alters inter-regional synchrony at both coarse (i.e. static

359    functional connectivity over longer time periods, in the range of minutes) and finer timescales

360    (i.e. functional changes within shorter time windows, in the range of seconds). In particular,

361    we find decreased localised activity (occipito-parietal, early visual) after training with anodal

362    stimulation, consistent with the decreased static occipito-parietal connectivity. In contrast, we

363    find increased widespread synchronised activation across the whole visual cortex after training

364    with anodal stimulation. Widespread synchronised activity has been linked to integration of

365    information (Varela et al., 2001) and higher sensitivity in error detection (Breakspear et al.,

366    2003). These processes are key for our signal-in-noise task that involves integrating

16

367    information across space, detecting the relevant features (i.e. signal) and suppressing irrelevant

368    information (i.e. noise).

369         Finally, despite the wide interest that tDCS has attracted in cognitive and clinical

370    neuroscience, its validity remains debated and our understanding of the tDCS mechanisms of

371    action remains limited (Fertonani and Miniussi, 2017). Here we address this challenge by

372    combining tDCS with brain imaging to interrogate the brain mechanisms that underlie the

373    facilitatory effect of tDCS on learning and brain plasticity. Our findings dissociate faster vs.

374    slower learning mechanisms and provide evidence for GABAergic plasticity mechanisms

375    across stages of learning. In particular, we demonstrate that tDCS results in faster learning to

376    detect targets in clutter by accelerating GABAergic plasticity (i.e. reducing GABAergic

377    inhibition) and decreasing occipito-parietal connectivity. Our findings propose that brain

378    stimulation during training optimises sensory processing through local gain control

379    mechanisms (i.e. reduction of GABAergic inhibition) (Katzner et al., 2011) to support

380    improved perceptual decisions (i.e. detecting targets in cluttered scenes).

381

**Materials and Methods**

**Participants**

384    We tested forty-five healthy volunteers (27 female; mean age 22.9 ± 3.3 years) in two

385    intervention groups, twenty-four in the stimulation group (Anodal) and twenty-one in the no-

386    stimulation group (Sham). We tested an additional no-intervention group of twenty-two healthy

387    volunteers who did not receive training nor stimulation (Control: 17 female; mean age 25.8 ±

388    4.2 years). All participants were right-handed, had normal or corrected-to-normal vision, did

389    not receive any prescription medication, were naïve to the aim of the study, gave written

390    informed consent and received payment for their participation. The study was approved by the

391    University of Cambridge Ethics Committee [PRE.2017.057].

17

**Stimuli**

We presented participants with Glass patterns (Glass, 1969) generated using previously described methods ((Zhang et al., 2010); Figure 1a). In particular, stimuli were defined by white dot pairs (dipoles) displayed within a square aperture on a black background. Stimuli (size=7.9$^o$ x 7.9$^o$), were presented in the left hemifield (11.6 arc min from fixation) contralateral to the stimulation site to ensure maximal effect of stimulation on stimulus processing. The dot density was 3%, and the Glass shift (i.e., the distance between two dots in a dipole) was 16.2 arc min. The size of each dot was 2.3 x 2.3 arc min$^2$. For each dot dipole, the spiral angle was defined as the angle between the dot dipole orientation and the radius from the centre of the dipole to the centre of the stimulus aperture. Each stimulus comprised dot dipoles that were aligned according to the specified spiral angle (signal dipoles) for a given stimulus and noise dipoles for which the spiral angle was randomly selected. The proportion of signal dipoles defined the stimulus signal level.

We generated radial (0$^o$ spiral angle) and concentric (90$^o$ spiral angle) Glass patterns by placing dipoles orthogonally (radial stimuli) or tangentially (concentric stimuli) to the circumference of a circle centred on the fixation dot. A new pattern was generated for each stimulus presented in a trial, resulting in stimuli that were locally jittered in their position. Radial (spiral angle: 0°) and concentric stimuli (spiral angle: ± 90°) were presented at 23% or 25% signal level counterbalanced across trials; noise dipoles were presented at random position and orientation. To control for potential local adaptation due to stimulus repetition and ensure that learning related to global shape rather than local stimulus features, we jittered (± 1-3°) the spiral angle across stimuli.

18

**Experimental Design**

415 

416 All participants in the intervention groups took part in a single brain imaging session during

417 which they were randomly assigned to the Anodal or Sham group. Participants in the Anodal

418 group received anodal tDCS on the right OCT, whereas participants in the Sham group did not

419 receive stimulation. We recorded three MRS measurements from the right OCT during

420 training: before, during and after stimulation. In addition, we recorded whole-brain rs-fMRI

421 data before and after training while participants fixated on a cross at the centre of the screen

422 (Figure 1b). Participants in the no-intervention Control group took part in a single brain

423 imaging session without stimulation or training; we recorded three MRS measurements from

424 right OCT at the same timings of the MRS measurements as for the intervention groups. We

425 did not record rs-fMRI data for this group due to time constraints.

426 During training, participants in the intervention groups were presented with Glass

427 patterns and were asked to judge and indicate by button press whether the presented stimulus

428 in each trial was radial or concentric. Two stimulus conditions (radial vs. concentric Glass

429 patterns; 100 trials per condition), were presented for each training block. For each trial, a

430 stimulus was presented for 300ms and was followed by fixation (i.e., blank screen with a central

431 fixation dot) while waiting for the participant's response (self-paced training paradigm). Trial-

432 by-trial feedback was provided by means of a visual cue (green tick for correct, red 'x' for

433 incorrect) followed by a fixation dot for 500ms before the onset of the next trial.

434 In the no-intervention control group, participants were tested in a contrast change

435 detection task. In particular, participants were presented with Glass patterns where 100% of the

436 dipoles were randomly oriented (0% signal patterns). In each trial, participants were asked to

437 choose whether the top or bottom half of the pattern underwent a contrast change. Task

438 difficulty was controlled by a two-up-one-down staircase to ensure participants were not

439 trained at the task and response accuracy was held at 75%.

**MRI data acquisition**

We collected MRI data on a 3T Siemens PRISMA scanner (Cognition and Brain Sciences Unit, Cambridge) using a 64-channel head coil. T1-weighted structural data (TR = 19.17s; TE = 2.31ms; number of slices = 176; voxel size = 1mm isotropic) and echo-planar imaging (EPI) data (gradient echo-pulse sequences) were acquired during rest (TR = 0.727s; TE = 34.6ms; number of slices = 72; voxel size = 2mm isotropic; Multi-band factor = 8; flip angle = 51°; number of volumes = 660; duration = 8m09s; whole brain coverage). During EPI data acquisition, we recorded cardiac pulsation (using a pulse oximeter) and respiration (using a respiratory belt) to model these physiological data for denoising.

**MRS data acquisition**

We collected MRS data with a MEGA-PRESS sequence (Mescher et al., 1998): echo time = 68ms, repetition time = 3000ms; 256 transients of 2048 data points were acquired in 13min experiment time; a 14.28ms Gaussian editing pulse was applied at 1.9 (ON) and 7.5 (OFF) ppm; water unsuppressed 16 transients (Table S6, following guidelines by (Lin et al., 2021)). Measurements with this sequence at 3T have been previously shown to produce reliable and reproducible estimates of GABA+ (Puts and Edden, 2012). Water suppression was achieved using variable power with optimized relaxation delays and outer volume suppression. Automated shimming was conducted to achieve water linewidth below 10Hz. We acquired spectra from an MRS voxel (20 x 20 x 25 mm$^3$) in the right OCT (Figure 3). We manually positioned the MRS voxel using anatomical landmarks (superior temporal gyrus, middle occipital gyrus) on each participant's structural scan, ensuring that voxel placement was consistent across participants. The centre of gravity for the MRS voxel was: x=40.8±3.2mm, y=-61.7±5.2mm, z=10.6±3.6mm in Montreal Neurological Institute (MNI) space. During the

20

464    MRS acquisitions, participants in the intervention groups performed the SN task, while

465    participants in the no-intervention control group performed the contrast change detection task.

466

**tDCS data acquisition**

468    We used a multi-channel transcranial electrical stimulator (neuroConn DC-STIMULATOR

469    MC, Ilmenau, Germany) to deliver anodal or sham stimulation. We used a pair of MR-

470    compatible rubber electrodes (3x3 cm$^2$ stimulating electrode, 5x5 cm$^2$ reference electrode),

471    which were secured on the head with the help of rubber bands. Ten-20 paste was used as a

472    conductive medium between the rubber electrodes and the scalp. For the Anodal group, 1mA

473    current was ramped up over 10s, was held at 1mA for 20min and was subsequently ramped

474    down over 10s. For the Sham group, the current ramped up (10s) and down (10s) in the

475    beginning of the session. We used online stimulation (i.e. stimulation during training), as this

476    protocol has been previously shown to enhance the lasting effect of training (O'Shea et al.,

477    2017). It has been shown that this facilitatory effect is not present or polarity-specific when

478    stimulation precedes training, with anodal stimulation impeding learning (Stagg et al., 2011).

479    To achieve consistent electrode placement across participants when targeting the right posterior

480    OCT (consistent with the MRS acquisition in the right OCT), we placed the bottom right corner

481    of the square stimulating electrode on T6, using a 10-20 system EEG cap, maintaining the same

482    orientation across participants, parallel to the line connecting T6 and O2. The reference

483    electrode was placed on Cz. We have previously used the same electrode montage (Frangou et

484    al, 2018), following electrical field density simulations showing that this montage results in

485    unilaterally localised current density, the peak of the electric field density being under the

486    anode electrode around the posterior OCT and the stimulation reaching the region where the

487    MRS voxel was placed.

488

**Behavioural data analysis**

We measured behavioural performance per training block as the mean accuracy per 200 trials. To quantify learning-dependent changes in behaviour, we computed the behavioural performance before, during and after stimulation as the average performance of blocks 1-2 (Pre), 3-5 (During) and 6-9 (Post), respectively. Further, we quantified learning rate by fitting individual participant training data with a logarithmic function: $y = k * \ln x + c$, where $x$ is the training run separated into 100 trial bins, $y$ is the run accuracy, $c$ is the starting performance and $k$ corresponds to the learning rate. Positive learning rate indicates that performance improved with training, whereas negative or close to zero learning rate indicates no behavioural improvement.

**MRS data analysis**

We pre-processed the MRS data using MRspa v1.5c (www.cmrr.umn.edu/downloads/mrspa/). We applied Eddy current, frequency and phase correction before subtracting the average ON and OFF spectra, resulting in edited spectra. We used LC-Model (Provencher, 2001) to quantify metabolite concentrations by fitting simulated model spectra of γ-amino-butyric acid (GABA), Glu, Glutamine and NAA to the edited spectra (Figure 3b), setting the sptype parameter to mega-press-2. We refer to GABA concentration as GABA+, as MRS measurements of GABA with MEGA-PRESS include co-edited macromolecules (Mullins et al., 2014). We referenced metabolite concentrations to the concentration of water for our analyses and then validated our findings by referencing GABA+ to NAA to ensure our results were not driven by the chosen reference (Lunghi et al., 2015).

GABA+ measurements within 3 standard deviations from the mean across all groups and blocks (data for 1 participant of the Anodal group were excluded) and with Cramer-Rao lower bound (CRLB) values smaller than 15% (data for 2 participants of the Anodal group and

514   1 of the Sham group were excluded) were included in further steps of MRS related analyses.

515   SNR was calculated as the amplitude of the NAA peak in the difference-spectrum divided by

516   twice the root mean square of the residual signal (Provencher, 2001). We report average quality

517   indices (CRLB, linewidth, SNR) per group and block (Table S1). To control for potential

518   differences in data quality across participants and blocks, we performed control analyses that

519   accounted for changes in linewidth and SNR (Table S2, Table S3). We did not include control

520   analyses for changes in CRLB, as reductions in GABA concentration have been shown to be

521   inherently linked to increases in CRLB (Emir et al., 2012; Kreis, 2016; Lunghi et al., 2015).

522   Further, we conducted whole brain tissue-type segmentation of the T1-weighted

523   structural scan and calculated percentage of grey matter, white matter and cerebrospinal fluid

524   (CSF) in the MRS voxel. To ensure that correlations with GABA+ were not driven by

525   variability in tissue composition within the MRS voxel across participants, we conducted two

526   control analyses (Table S2, Table S3): (a) regressed out the CSF percentage from the GABA+

527   concentrations, (b) applied α-correction on the GABA+ values to account for the difference in

528   GABA+ between grey and white matter (Porges et al., 2017).

529

530   **rs-fMRI data analysis**

531   We pre-processed the structural and the rs-fMRI data in SPM12.4 (v7219;

532   www.fil.ion.ucl.ac.uk/spm/software/spm12/) following the Human Connectome Project

533   pipeline for multi-band data (Smith et al., 2013). In particular, we first coregistered (non-

534   linearly) the T1w structural images (after brain extraction) to MNI space to ensure that all

535   participant data were in the same stereotactic space for statistical analysis. We then (a)

536   corrected the EPI data for susceptibility distortions (fieldmap correction) and any spatial

537   misalignments between EPI volumes due to head movement (i.e. aligned each run to its single

538   band reference image), (b) coregistered the second EPI run to the first (rigid body) to correct

23

539　any spatial misalignments between runs, (c) coregistered the first EPI run to the structural

540　image (rigid body) and (d) normalised them to MNI space for subsequent statistical analyses

541　(applying the deformation field of the structural images). Data were only resliced after MNI

542　normalisation to minimise the number of interpolation steps. Following MNI normalisation,

543　(e) data were skull-stripped, (f) spatially smoothed with a 4mm Gaussian kernel to improve the

544　signal-to-noise ratio and the alignment between participant data (two times the voxel size;

545　(Chen and Calhoun, 2018)), (g) wavelet despiked to remove any secondary motion artifacts

546　(Patel et al., 2014) and (h) had linear drifts removed (linear detrending due to scanner noise).

547　Slice-timing correction was not applied, following previous work on fast TR (sub-second)

548　acquisition protocols (Smith et al., 2013). Data from 8 participants (2 anodal, 6 sham) were

549　excluded from further analysis due to missing the second rs-fMRI run.

550　　Next, we applied spatial group Independent Component Analysis (ICA) using the

551　Group ICA fMRI Toolbox (GIFT v3.0b) (http://mialab.mrn.org/software/gift/) to identify and

552　remove components of noise. PCA was applied for dimensionality reduction, first at the subject

553　level, then at the group level. The Minimum Description Length criteria (Rissanen, 1978) were

554　used to estimate the dimensionality and determine the number of independent components. The

555　ICA estimation (Infomax) was run 20 times and the component stability was estimated using

556　ICASSO (Himberg et al., 2004). Following recent work on back-reconstruction methods for

557　ICA denoising at the group level (Du et al., 2016), we used Group Information Guided ICA

558　(GIG-ICA) back-reconstruction to reconstruct subject-specific components from the group

559　components. We visually inspected the results and identified noise components according to

560　published procedures (Griffanti et al., 2017). Using consensus voting among 3 experts, we

561　labelled 8 of the 31 components as noise that captured signal from veins, arteries, CSF

562　pulsation, susceptibility and multi-band artefacts.

563    To clean the fMRI signals from signals related to motion and the noise components, we

564    followed a soft clean-up ICA denoise approach (Griffanti et al., 2014). That is, we first

565    regressed out the motion parameters (translation, rotation and their squares and derivatives;

566    (Friston et al., 1996)) from each voxel and ICA component time course. Second, we estimated

567    the contribution of every ICA component to each voxel's time course (multiple regression).

568    Finally, we subtracted the unique contribution of the noise components from each voxel's time

569    course to avoid removing any shared signal between neuronal and noise components.

570    Following ICA denoise, we performed a first-level analysis modelling the physiological

571    data as nuisance variables. We used the TAPAS toolbox (Kasper et al., 2017) to create

572    physiological covariates that model terms for RETROICOR (Glover et al., 2000), heart rate

573    variability (Chang et al., 2009) and respiratory volume per time (Birn et al., 2008). Following

574    previous work (Caballero-Gaudes and Reynolds, 2017), we selected a second-order model for

575    both the cardiac and the respiratory signal (no interaction term) and zero delay for the heart

576    rate variability and respiratory volume per time terms. Within the GLM, the data were high-

577    pass filtered at 0.01Hz and treated for serial correlations using the FAST autoregressive model,

578    as it has been shown to perform more accurate autocorrelation modelling for fast TR

579    acquisitions (Corbin et al., 2018; Olszowy et al., 2019). The residual time course from the last

580    step was used for all subsequent analyses.

581

582    **Static connectivity analysis**

583    We calculated extrinsic functional connectivity between OCT and IPS and intrinsic

584    connectivity within OCT. First, we created masks for these two regions of interest (ROI). For

585    OCT, we computed the overlap across participant MRS voxels and created a group MRS mask

586    that included voxels present in at least 50% of the participants' MRS voxels. For IPS, we

25

587   created an equally sized cubic mask centred on the intraparietal cortex (centre at 34, -50, 42 in

588   MNI space (Frangou et al., 2019), edge length = 20mm).

589         Then, for each participant and ROI, we computed the first eigenvariate across all grey

590   matter voxels within the region to derive a single representative time course per ROI. We

591   applied a 5th order Butterworth band-pass filter between 0.01 and 0.08 Hz on the eigenvariate

592   time course, similar to previous studies (Cordes et al., 2001; Frangou et al., 2019; Murphy et

593   al., 2013). Extrinsic functional connectivity was computed as the Pearson correlation of the

594   OCT-IPS time courses. Similarly, intrinsic connectivity was computed as the Pearson

595   correlation of each OCT voxel's time course to the eigenvariate time course and then averaged

596   across voxels (Bachtiar et al., 2015; Frangou et al., 2019; Stagg et al., 2014; Van Dijk et al.,

597   2010). We computed the change in rs-fMRI connectivity as the difference of the pre- from the

598   post-intervention run (after Fisher z-transform) and tested for: (a) changes in extrinsic and

599   intrinsic connectivity, (b) correlations of connectivity change with OCT GABA+ change, and

600   (c) correlations of connectivity change with behaviour. For correlations with GABA+ and

601   behaviour, we regressed out the pre-intervention connectivity from the difference to control for

602   baseline differences across participants.

603

604   **Time-varying connectivity analysis**

605   We estimated time-varying functional connectivity using the HMM-MAR toolbox (Vidaurre

606   et al., 2018, 2017). In particular, we estimated a HMM on the visual cortex to detect brain states

607   representing recurrent patterns of activity and connectivity over time. Using a Bayesian

608   approach, the model learns a set of parameters for each state and the probability of their

609   activation at each time point given the recorded data. Specifically, given an active state $Z_t$ at

610   time $t$, the recorded data sample $X_t$ is described by a multivariate Gaussian distribution:

26

611    $P(X_t|Z_t = k) \sim N(\mu_k, \Sigma_k)$. Each state has distinct mean and covariance parameters that

612    capture each state's mean activation and functional connectivity.

613      To investigate the dynamics of the occipito-parietal (OCT-IPS) interactions with the

614    rest of the visual cortex, we defined fourteen bilateral regions from the Probabilistic map of

615    Visual Topography (Wang et al., 2015) (Table S4). We then computed the first eigenvariate

616    across all voxels within each region to derive a single representative time course per ROI. We

617    concatenated the time courses of all ROIs across participants and runs to estimate state

618    distributions (i.e. the spatial parameters of the model) at the group level, whereas the

619    probability of a state activation is still defined uniquely for each timepoint at the participant

620    level (i.e. the temporal parameters of the model; (Vidaurre et al., 2016)).

621      Latent variable models (such as the HMM) can be sensitive to local minima or poor

622    initialisation (Vidaurre et al., 2019). To ensure stability on the estimation of the HMM states,

623    we ran the algorithm 10 times with 10 random initialisations for each iteration and selected the

624    iteration with the lowest free energy for simplicity. Further, we tested whether the results were

625    robust to variations of key hyperparameters: the number of states ranging from 4 to 10, and the

626    input data dimensionality by varying the number of retained PCA dimensions to capture

627    between 70% and 100% of the variance (in increments of 10%).

628      To describe the state dynamics, we computed two summary measures: FO per state, as

629    the proportion of time spent in that state, and SR across states, as the frequency of switching

630    between states. That is, a state with increased (decreased) FO after training indicates that

631    regions within that state are more (less) involved in the processing of the task, suggesting a

632    higher (lower) engagement of that state after training. Similarly, increased SR after training

633    indicates faster switching from one state to another over time, suggesting shorter processing

634    times within a state after training. Finally, we computed change in FO and SR as the difference

635    of the pre- from the post-intervention rs-fMRI run and tested for within-group changes.

27

**Statistical analysis**

For ANOVAs, we tested for sphericity and used Greenhouse-Geisser (for epsilon less than 0.75) or Huynh-Feldt (for epsilon greater than 0.75) correction, if sphericity was violated. For correlational analyses, we used skipped Pearson correlation of the Robust Correlation Toolbox to account for bivariate outliers and adjusted the degrees of freedom when outliers were detected (Pernet et al., 2013).

657 **References**

658 Antal A, Kincses TZ, Nitsche MA, Bartfai O, Paulus W. 2004a. Excitability Changes

659       Induced in the Human Primary Visual Cortex by Transcranial Direct Current

660       Stimulation: Direct Electrophysiological Evidence. *Investig Opthalmology Vis Sci*

661       **45**:702. doi:10.1167/iovs.03-0688

662 Antal A, Nitsche MA, Kruse W, Kincses TZ, Hoffmann K-P, Paulus W. 2004b. Direct

663       Current Stimulation over V5 Enhances Visuomotor Coordination by Improving Motion

664       Perception in Humans. *J Cogn Neurosci* **16**:521–527.

665       doi:10.1162/089892904323057263

666 Antonenko D, Schubert F, Bohm F, Ittermann B, Aydin S, Hayek D, Grittner U, Flöel A.

667       2017. tDCS-Induced Modulation of GABA Levels and Resting-State Functional

668       Connectivity in Older Adults. *J Neurosci* **37**:4065–4073.

669       doi:10.1523/JNEUROSCI.0079-17.2017

670 Bachtiar V, Near J, Johansen-Berg H, Stagg CJ. 2015. Modulation of GABA and resting state

671       functional connectivity by transcranial direct current stimulation. *Elife* **4**:1–9.

672       doi:10.7554/eLife.08789

673 Barron HC, Vogels TP, Emir UE, Makin TR, O'Shea J, Clare S, Jbabdi S, Dolan RJ, Behrens

674       TEJ. 2016. Unmasking Latent Inhibitory Connections in Human Cortex to Reveal

675       Dormant Cortical Memories. *Neuron*. doi:10.1016/j.neuron.2016.02.031

676 Battaglini L, Noventa S, Casco C. 2017. Anodal and cathodal electrical stimulation over V5

677       improves motion perception by signal enhancement and noise reduction. *Brain Stimul*

678       **10**:773–779. doi:10.1016/j.brs.2017.04.128

679 Birn RM, Smith MA, Jones TB, Bandettini PA. 2008. The respiration response function: The

680       temporal dynamics of fMRI signal fluctuations related to changes in respiration.

681       *Neuroimage* **40**:644–654. doi:10.1016/j.neuroimage.2007.11.059

682   Breakspear M, Terry JR, Friston KJ. 2003. Modulation of excitatory synaptic coupling

683      facilitates synchronization and complex dynamics in a biophysical model of neuronal

684      dynamics. *Netw Comput Neural Syst* **14**:703–732. doi:10.1088/0954-898X_14_4_305

685   Caballero-Gaudes C, Reynolds RC. 2017. Methods for cleaning the BOLD fMRI signal.

686      *Neuroimage* **154**:128–149. doi:10.1016/j.neuroimage.2016.12.018

687   Calhoun VD, Miller R, Pearlson G, Adali T. 2014. The Chronnectome: Time-Varying

688      Connectivity Networks as the Next Frontier in fMRI Data Discovery. *Neuron* **84**:262–

689      274. doi:10.1016/j.neuron.2014.10.015

690   Callan DE, Falcone B, Wada A, Parasuraman R. 2016. Simultaneous tDCS-fMRI identifies

691      resting state networks correlated with visual search enhancement. *Front Hum Neurosci*

692      **10**:1–12. doi:10.3389/fnhum.2016.00072

693   Cao J, Liu H. 2018. Modulating the resting-state functional connectivity patterns of language

694      processing areas in the human brain with anodal transcranial direct current stimulation

695      applied over the Broca's area. *Neurophotonics* **5**:1. doi:10.1117/1.nph.5.2.025002

696   Chang C, Cunningham JP, Glover GH. 2009. Influence of heart rate on the BOLD signal:

697      The cardiac response function. *Neuroimage* **44**:857–869.

698      doi:10.1016/j.neuroimage.2008.09.029

699   Chang DHF, Mevorach C, Kourtzi Z, Welchman AE. 2014. Training transfers the limits on

700      perception from parietal to ventral cortex. *Curr Biol*. doi:10.1016/j.cub.2014.08.058

701   Chen Z, Calhoun V. 2018. Effect of Spatial Smoothing on Task fMRI ICA and Functional

702      Connectivity. *Front Neurosci* **12**:15. doi:10.3389/fnins.2018.00015

703   Cohen JR. 2017. The behavioral and cognitive relevance of time-varying, dynamic changes

704      in functional connectivity. *Neuroimage* 1–11. doi:10.1016/j.neuroimage.2017.09.036

705   Corbin N, Todd N, Friston KJ, Callaghan MF. 2018. Accurate modeling of temporal

706      correlations in rapidly sampled fMRI time series. *Hum Brain Mapp* **39**:3884–3897.

30

707      doi:10.1002/hbm.24218

708      Cordes D, Haughton VM, Arfanakis K, Carew JD, Turski PA, Moritz CH, Quigley MA,

709      Meyerand ME. 2001. Frequencies contributing to functional connectivity in the cerebral

710      cortex in "resting-state" data. *Am J Neuroradiol* **22**:1326–1333.

711      Du Y, Allen EA, He H, Sui J, Wu L, Calhoun VD. 2016. Artifact removal in the context of

712      group ICA: A comparison of single-subject and group approaches. *Hum Brain Mapp*

713      **37**:1005–1025. doi:10.1002/hbm.23086

714      Eichenbaum A, Pappas I, Lurie D, Cohen JR, D'Esposito M. 2021. Differential contributions

715      of static and time-varying functional connectivity to human behavior. *Netw Neurosci*

716      **5**:145–165. doi:10.1162/netn_a_00172

717      Emir UE, Tuite PJ, Öz G. 2012. Elevated pontine and putamenal gaba levels in mild-

718      moderate parkinson disease detected by 7 tesla proton mrs. *PLoS One*.

719      doi:10.1371/journal.pone.0030918

720      Fertonani A, Miniussi C. 2017. Transcranial Electrical Stimulation. *Neurosci* **23**:109–123.

721      doi:10.1177/1073858416631966

722      Frangou P, Correia M, Kourtzi Z. 2018. GABA, not BOLD, reveals dissociable learning-

723      dependent plasticity mechanisms in the human brain. *Elife* **7**:1–22.

724      doi:10.7554/eLife.35854

725      Frangou P, Emir UE, Karlaftis VM, Nettekoven C, Hinson EL, Larcombe S, Bridge H, Stagg

726      CJ, Kourtzi Z. 2019. Learning to optimize perceptual decisions through suppressive

727      interactions in the human brain. *Nat Commun 2019 101* **10**:474. doi:10.1038/s41467-

728      019-08313-y

729      Friston KJ, Williams S, Howard R, Frackowiak RSJ, Turner R. 1996. Movement-Related

730      effects in fMRI time-series. *Magn Reson Med* **35**:346–355.

731      doi:10.1002/mrm.1910350312

732    Glass L. 1969. Moiré effect from random dots. *Nature*. doi:10.1038/223578a0

733    Glover GH, Li T, Ress D. 2000. Image-based method for retrospective correction of

734        physiological motion effects in fMRI: RETROICOR. *Magn Reson Med* **44**:162–167.

735        doi:10.1002/1522-2594(200007)44:1<162::aid-mrm23>3.3.co;2-5

736    Griffanti L, Douaud G, Bijsterbosch J, Evangelisti S, Alfaro-Almagro F, Glasser MF, Duff

737        EP, Fitzgibbon S, Westphal R, Carone D, Beckmann CF, Smith SM. 2017. Hand

738        classification of fMRI ICA noise components. *Neuroimage* **154**:188–205.

739        doi:10.1016/j.neuroimage.2016.12.036

740    Griffanti L, Salimi-Khorshidi G, Beckmann CF, Auerbach EJ, Douaud G, Sexton CE,

741        Zsoldos E, Ebmeier KP, Filippini N, Mackay CE, Moeller S, Xu J, Yacoub E, Baselli G,

742        Ugurbil K, Miller KL, Smith SM. 2014. ICA-based artefact removal and accelerated

743        fMRI acquisition for improved resting state network imaging. *Neuroimage* **95**:232–247.

744        doi:10.1016/j.neuroimage.2014.03.034

745    Guerra-Carrillo B, Mackey AP, Bunge SA. 2014. Resting-State fMRI: A Window into

746        Human Brain Plasticity. *Neurosci* **20**:522–533. doi:10.1177/1073858414524442

747    Harris AD, Wang Z, Ficek B, Webster K, Edden RA, Tsapkini K. 2019. Reductions in

748        GABA following a tDCS-language intervention for primary progressive aphasia.

749        *Neurobiol Aging* **79**:75–82. doi:10.1016/j.neurobiolaging.2019.03.011

750    Himberg J, Hyvärinen A, Esposito F. 2004. Validating the independent components of

751        neuroimaging time series via clustering and visualization. *Neuroimage* **22**:1214–1222.

752        doi:10.1016/j.neuroimage.2004.03.027

753    Hutchison RM, Womelsdorf T, Allen EA, Bandettini PA, Calhoun VD, Corbetta M, Della

754        Penna S, Duyn JH, Glover GH, Gonzalez-Castillo J, Handwerker DA, Keilholz S,

755        Kiviniemi V, Leopold DA, de Pasquale F, Sporns O, Walter M, Chang C. 2013.

756        Dynamic functional connectivity: Promise, issues, and interpretations. *Neuroimage*

757    **80**:360–378. doi:10.1016/j.neuroimage.2013.05.079

758    Ip IB, Bridge H. 2021. Investigating the neurochemistry of the human visual system using

759    magnetic resonance spectroscopy. *Brain Struct Funct* **1**:3. doi:10.1007/s00429-021-

760    02273-0

761    Kapogiannis D, Reiter DA, Willette AA, Mattson MP. 2013. Posteromedial cortex glutamate

762    and GABA predict intrinsic functional connectivity of the default mode network.

763    *Neuroimage*. doi:10.1016/j.neuroimage.2012.09.029

764    Karapanagiotidis T, Vidaurre D, Quinn AJ, Vatansever D, Poerio GL, Turnbull A, Ho NSP,

765    Leech R, Bernhardt BC, Jefferies E, Margulies DS, Nichols TE, Woolrich MW,

766    Smallwood J. 2020. The psychological correlates of distinct neural states occurring

767    during wakeful rest. *Sci Rep* **10**:21121. doi:10.1038/s41598-020-77336-z

768    Karlaftis VM, Giorgio J, Vértes PE, Wang R, Shen Y, Tino P, Welchman AE, Kourtzi Z.

769    2019. Multimodal imaging of brain connectivity reveals predictors of individual

770    decision strategy in statistical learning. *Nat Hum Behav* **3**:297–307. doi:10.1038/s41562-

771    018-0503-4

772    Karlaftis VM, Giorgio J, Zamboni E, Frangou P, Rideaux R, Ziminski JJ, Kourtzi Z. 2021.

773    Functional Interactions between Sensory and Memory Networks for Adaptive Behavior.

774    *Cereb Cortex* 1–12. doi:10.1093/cercor/bhab160

775    Kasper L, Bollmann S, Diaconescu AO, Hutton C, Heinzle J, Iglesias S, Hauser TU, Sebold

776    M, Manjaly ZM, Pruessmann KP, Stephan KE. 2017. The PhysIO Toolbox for

777    Modeling Physiological Noise in fMRI Data. *J Neurosci Methods* **276**:56–72.

778    doi:10.1016/j.jneumeth.2016.10.019

779    Katzner S, Busse L, Carandini M. 2011. GABAA Inhibition Controls Response Gain in

780    Visual Cortex. *J Neurosci* **31**:5931–5941. doi:10.1523/JNEUROSCI.5753-10.2011

781    Kelly C, Castellanos FX. 2014. Strengthening connections: Functional connectivity and brain

782    plasticity. *Neuropsychol Rev* **24**:63–76. doi:10.1007/s11065-014-9252-y

783    Kolasinski J, Hinson EL, Divanbeighi Zand AP, Rizov A, Emir UE, Stagg CJ. 2019. The

784        dynamics of cortical GABA in human motor learning. *J Physiol*. doi:10.1113/JP276626

785    Krause MR, Zanos TP, Csorba BA, Pilly PK, Choe J, Phillips ME, Datta A, Pack CC. 2017.

786        Transcranial Direct Current Stimulation Facilitates Associative Learning and Alters

787        Functional Connectivity in the Primate Brain. *Curr Biol* **27**:3086-3096.e3.

788        doi:10.1016/j.cub.2017.09.020

789    Kreis R. 2016. The trouble with quality filtering based on relative Cramér-Rao lower bounds.

790        *Magn Reson Med* **75**:15–18. doi:10.1002/mrm.25568

791    Krishnamurthy V, Gopinath K, Brown GS, Hampstead BM. 2015. Resting-state fMRI reveals

792        enhanced functional connectivity in spatial navigation networks after transcranial direct

793        current stimulation. *Neurosci Lett* **604**:80–85. doi:10.1016/j.neulet.2015.07.042

794    Lewis CM, Baldassarre A, Committeri G, Romani GL, Corbetta M. 2009. Learning sculpts

795        the spontaneous activity of the resting human brain. *Proc Natl Acad Sci* **106**:17558–

796        17563. doi:10.1073/pnas.0902455106

797    Liégeois R, Li J, Kong R, Orban C, Van De Ville D, Ge T, Sabuncu MR, Yeo BTT. 2019.

798        Resting brain dynamics at different timescales capture distinct aspects of human

799        behavior. *Nat Commun* **10**:2317. doi:10.1038/s41467-019-10317-7

800    Lin A, Andronesi O, Bogner W, Choi I, Coello E, Cudalbu C, Juchem C, Kemp GJ, Kreis R,

801        Krššák M, Lee P, Maudsley AA, Meyerspeer M, Mlynarik V, Near J, Öz G, Peek AL,

802        Puts NA, Ratai E, Tkáč I, Mullins PG. 2021. Minimum Reporting Standards for in vivo

803        Magnetic Resonance Spectroscopy (MRSinMRS): Experts' consensus

804        recommendations. *NMR Biomed* **34**:e4484. doi:10.1002/nbm.4484

805    Lunghi C, Emir UE, Morrone MC, Bridge H. 2015. Short-Term Monocular Deprivation

806        Alters GABA in the Adult Human Visual Cortex. *Curr Biol* **25**:1496–1501.

807      doi:10.1016/j.cub.2015.04.021

808    Mann EO, Paulsen O. 2007. Role of GABAergic inhibition in hippocampal network

809      oscillations. *Trends Neurosci* **30**:343–349. doi:10.1016/j.tins.2007.05.003

810    Mayhew SD, Li S, Kourtzi Z. 2012. Learning acts on distinct processes for visual form

811      perception in the human brain. *J Neurosci*. doi:10.1523/JNEUROSCI.2033-11.2012

812    McDermott TJ, Wiesman AI, Mills MS, Spooner RK, Coolidge NM, Proskovec AL,

813      Heinrichs-Graham E, Wilson TW. 2019. tDCS modulates behavioral performance and

814      the neural oscillatory dynamics serving visual selective attention. *Hum Brain Mapp*

815      **40**:729–740. doi:10.1002/hbm.24405

816    Meinzer M, Antonenko D, Lindenberg R, Hetzer S, Ulm L, Avirame K, Flaisch T, Flöel A.

817      2012. Electrical brain stimulation improves cognitive performance by modulating

818      functional connectivity and task-specific activation. *J Neurosci* **32**:1859–1866.

819      doi:10.1523/JNEUROSCI.4812-11.2012

820    Mescher M, Merkle H, Kirsch J, Garwood M, Gruetter R. 1998. Simultaneous in vivo

821      spectral editing and water suppression. *NMR Biomed* **11**:266–272.

822      doi:10.1002/(SICI)1099-1492(199810)11:6<266::AID-NBM530>3.0.CO;2-J

823    Mullins PG, McGonigle DJ, O'Gorman RL, Puts NAJ, Vidyasagar R, Evans CJ, Edden RAE.

824      2014. Current practice in the use of MEGA-PRESS spectroscopy for the detection of

825      GABA. *Neuroimage* **86**:43–52. doi:10.1016/j.neuroimage.2012.12.004

826    Murphy K, Birn RM, Bandettini PA. 2013. Resting-state fMRI confounds and cleanup.

827      *Neuroimage* **80**:349–359. doi:10.1016/j.neuroimage.2013.04.001

828    Nasrallah FA, Singh KKD /O. R, Yeow LY, Chuang K-H. 2017. GABAergic effect on

829      resting-state functional connectivity: Dynamics under pharmacological antagonism.

830      *Neuroimage* **149**:53–62. doi:10.1016/j.neuroimage.2017.01.040

831    Nitsche MA, Paulus W. 2000. Excitability changes induced in the human motor cortex by

832    weak transcranial direct current stimulation. *J Physiol*. doi:10.1111/j.1469-

833    7793.2000.t01-1-00633.x

834    O'Shea J, Revol P, Cousijn H, Near J, Petitet P, Jacquin-Courtois S, Berg HJ, Rode G,

835    Rossetti Y. 2017. Induced sensorimotor cortex plasticity remediates chronic treatment-

836    resistant visual neglect. *Elife*. doi:10.7554/eLife.26602

837    Olszowy W, Aston J, Rua C, Williams GB. 2019. Accurate autocorrelation modeling

838    substantially improves fMRI reliability. *Nat Commun* **10**:1–12. doi:10.1038/s41467-

839    019-09230-w

840    Patel AX, Kundu P, Rubinov M, Jones PS, Vértes PE, Ersche KD, Suckling J, Bullmore ET.

841    2014. A wavelet method for modeling and despiking motion artifacts from resting-state

842    fMRI time series. *Neuroimage* **95**:287–304. doi:10.1016/j.neuroimage.2014.03.012

843    Pernet CR, Wilcox R, Rousselet GA. 2013. Robust Correlation Analyses: False Positive and

844    Power Validation Using a New Open Source Matlab Toolbox. *Front Psychol* **3**.

845    doi:10.3389/fpsyg.2012.00606

846    Porges EC, Woods AJ, Lamb DG, Williamson JB, Cohen RA, Edden RAE, Harris AD. 2017.

847    Impact of tissue correction strategy on GABA-edited MRS findings. *Neuroimage*

848    **162**:249–256. doi:10.1016/j.neuroimage.2017.08.073

849    Preti MG, Bolton TA, Van De Ville D. 2017. The dynamic functional connectome: State-of-

850    the-art and perspectives. *Neuroimage* **160**:41–54. doi:10.1016/j.neuroimage.2016.12.061

851    Provencher SW. 2001. Automatic quantitation of localizedin vivo1H spectra with LCModel.

852    *NMR Biomed* **14**:260–264. doi:10.1002/nbm.698

853    Puts NAJ, Edden RAE. 2012. In vivo magnetic resonance spectroscopy of GABA: A

854    methodological review. *Prog Nucl Magn Reson Spectrosc* **60**:29–41.

855    doi:10.1016/j.pnmrs.2011.06.001

856    Rissanen J. 1978. Modeling by shortest data description. *Automatica* **14**:465–471.

857     doi:10.1016/0005-1098(78)90005-5

858     Sampaio-Baptista C, Filippini N, Stagg CJ, Near J, Scholz J, Johansen-Berg H. 2015.

859     Changes in functional connectivity and GABA levels with long-term motor learning.

860     *Neuroimage*. doi:10.1016/j.neuroimage.2014.11.032

861     Sczesny-Kaiser M, Beckhaus K, Dinse HR, Schwenkreis P, Tegenthoff M, Höffken O. 2016.

862     Repetitive Transcranial Direct Current Stimulation Induced Excitability Changes of

863     Primary Visual Cortex and Visual Learning Effects—A Pilot Study. *Front Behav*

864     *Neurosci* **10**:116. doi:10.3389/fnbeh.2016.00116

865     Shibata K, Sasaki Y, Bang JW, Walsh EG, Machizawa MG, Tamaki M, Chang L-H,

866     Watanabe T. 2017. Overlearning hyperstabilizes a skill by rapidly making

867     neurochemical processing inhibitory-dominant. *Nat Neurosci* **20**:470–475.

868     doi:10.1038/nn.4490

869     Shmuel A, Leopold DA. 2008. Neuronal correlates of spontaneous fluctuations in fMRI

870     signals in monkey visual cortex: Implications for functional connectivity at rest. *Hum*

871     *Brain Mapp*. doi:10.1002/hbm.20580

872     Smith SM, Beckmann CF, Andersson J, Auerbach EJ, Bijsterbosch J, Douaud G, Duff E,

873     Feinberg DA, Griffanti L, Harms MP, Kelly M, Laumann T, Miller KL, Moeller S,

874     Petersen S, Power J, Salimi-Khorshidi G, Snyder AZ, Vu AT, Woolrich MW, Xu J,

875     Yacoub E, Uğurbil K, Van Essen DC, Glasser MF. 2013. Resting-state fMRI in the

876     Human Connectome Project. *Neuroimage* **80**:144–168.

877     doi:10.1016/j.neuroimage.2013.05.039

878     Spiegel DP, Byblow WD, Hess RF, Thompson B. 2013. Anodal Transcranial Direct Current

879     Stimulation Transiently Improves Contrast Sensitivity and Normalizes Visual Cortex

880     Activation in Individuals With Amblyopia. *Neurorehabil Neural Repair* **27**:760–769.

881     doi:10.1177/1545968313491006

882     Stagg CJ, Bachtiar V, Amadi U, Gudberg CA, Ilie AS, Sampaio-Baptista C, O'Shea J,

883         Woolrich M, Smith SM, Filippini N, Near J, Johansen-Berg H. 2014. Local GABA

884         concentration is related to network-level resting functional connectivity. *Elife* **3**:1–9.

885         doi:10.7554/eLife.01465

886     Stagg CJ, Best JG, Stephenson MC, O'Shea J, Wylezinska M, Kineses ZT, Morris PG,

887         Matthews PM, Johansen-Berg H. 2009. Polarity-sensitive modulation of cortical

888         neurotransmitters by transcranial stimulation. *J Neurosci*.

889         doi:10.1523/JNEUROSCI.4432-08.2009

890     Stagg CJ, Jayaram G, Pastor D, Kincses ZT, Matthews PM, Johansen-Berg H. 2011. Polarity

891         and timing-dependent effects of transcranial direct current stimulation in explicit motor

892         learning. *Neuropsychologia* **49**:800–804. doi:10.1016/j.neuropsychologia.2011.02.009

893     Van Dijk KR a, Hedden T, Venkataraman A, Evans KC, Lazar SW, Buckner RL. 2010.

894         Intrinsic Functional Connectivity As a Tool For Human Connectomics: Theory,

895         Properties, and Optimization. *J Neurophysiol* **103**:297–321. doi:10.1152/jn.00783.2009

896     Van Meel C, Daniels N, de Beeck HO, Baeck A. 2016. Effect of tDCS on task relevant and

897         irrelevant perceptual learning of complex objects. *J Vis* **16**:13. doi:10.1167/16.6.13

898     Varela F, Lachaux JP, Rodriguez E, Martinerie J. 2001. The brainweb: Phase synchronization

899         and large-scale integration. *Nat Rev Neurosci* **2**:229–239. doi:10.1038/35067550

900     Vidaurre D, Abeysuriya R, Becker R, Quinn AJ, Alfaro-Almagro F, Smith SM, Woolrich

901         MW. 2018. Discovering dynamic brain networks from big data in rest and task.

902         *Neuroimage* **180**:646–656. doi:10.1016/j.neuroimage.2017.06.077

903     Vidaurre D, Llera A, Smith SM, Woolrich MW. 2021. Behavioural relevance of spontaneous,

904         transient brain network interactions in fMRI. *Neuroimage* **229**:117713.

905         doi:10.1016/j.neuroimage.2020.117713

906     Vidaurre D, Quinn AJ, Baker AP, Dupret D, Tejero-Cantero A, Woolrich MW. 2016.

907      Spectrally resolved fast transient brain states in electrophysiological data. *Neuroimage*

908      **126**:81–95. doi:10.1016/j.neuroimage.2015.11.047

909   Vidaurre D, Smith SM, Woolrich MW. 2017. Brain network dynamics are hierarchically

910      organized in time. *Proc Natl Acad Sci* **114**:12827–12832. doi:10.1073/pnas.1705120114

911   Vidaurre D, Woolrich MW, Winkler AM, Karapanagiotidis T, Smallwood J, Nichols TE.

912      2019. Stable between-subject statistical inference from unstable within-subject

913      functional connectivity estimates. *Hum Brain Mapp* **40**:1234–1243.

914      doi:10.1002/hbm.24442

915   Wang L, Mruczek REB, Arcaro MJ, Kastner S. 2015. Probabilistic Maps of Visual

916      Topography in Human Cortex. *Cereb Cortex* **25**:3911–31. doi:10.1093/cercor/bhu277

917   Zhang J, Meeson A, Welchman AE, Kourtzi Z. 2010. Learning alters the tuning of functional

918      magnetic resonance imaging patterns for visual forms. *J Neurosci*.

919      doi:10.1523/JNEUROSCI.2204-10.2010

920   Zito G, Senti T, Cazzoli D, Müri R, Mosimann U, Nyffeler T, Nef T. 2015. Cathodal HD-

921      tDCS on the right V5 improves motion perception in humans   . *Front Behav Neurosci*  .

922

**Figures**
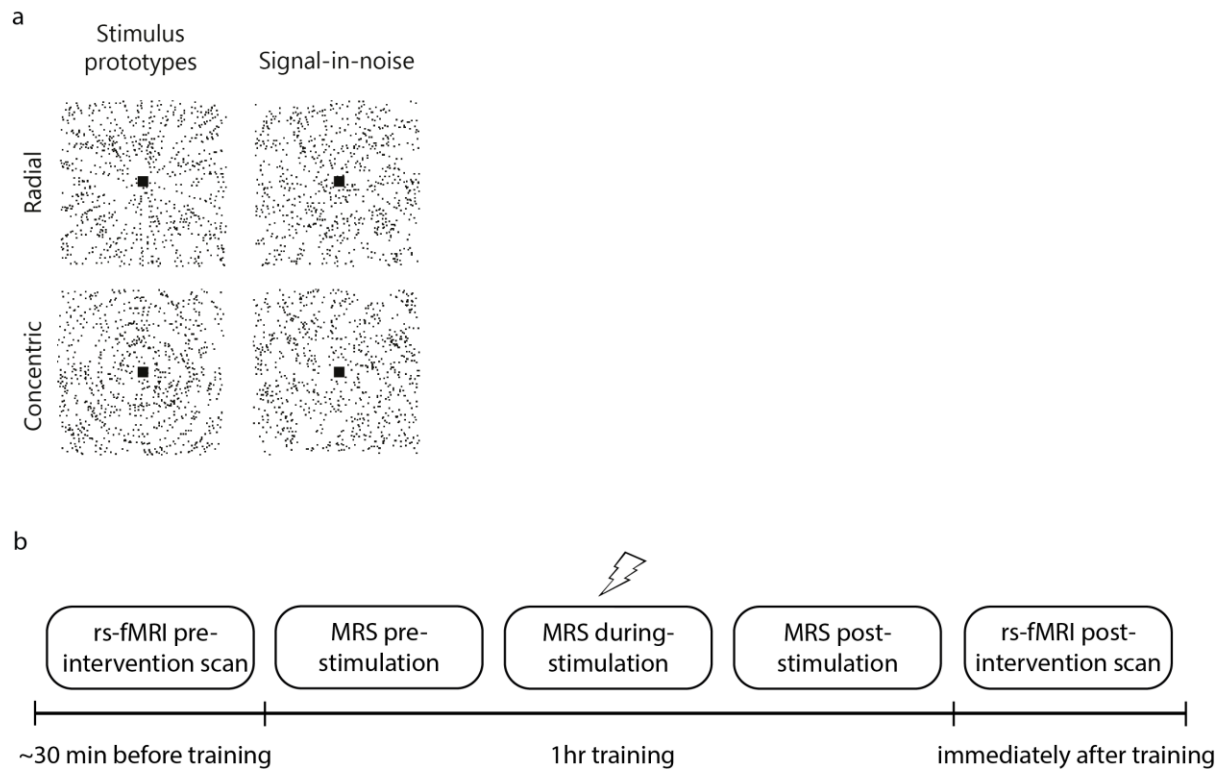


**Figure 1. Stimuli and experiment timeline**: (a) Example stimuli comprising radial and concentric Glass patterns (stimuli are presented with inverted contrast for illustration purposes). Stimuli are shown for the signal-in-noise task (25% signal, spiral angle 0° for radial and 90° for concentric). Prototype stimuli (100% signal, spiral angle 0° for radial and 90° for concentric) are shown for illustration purposes only. (b) Timeline of the experiment that comprises two rs-fMRI scans and three MRS measurements during training on the signal-in-noise task. tDCS was delivered during the second MRS acquisition for the intervention groups (Anodal, Sham).

40
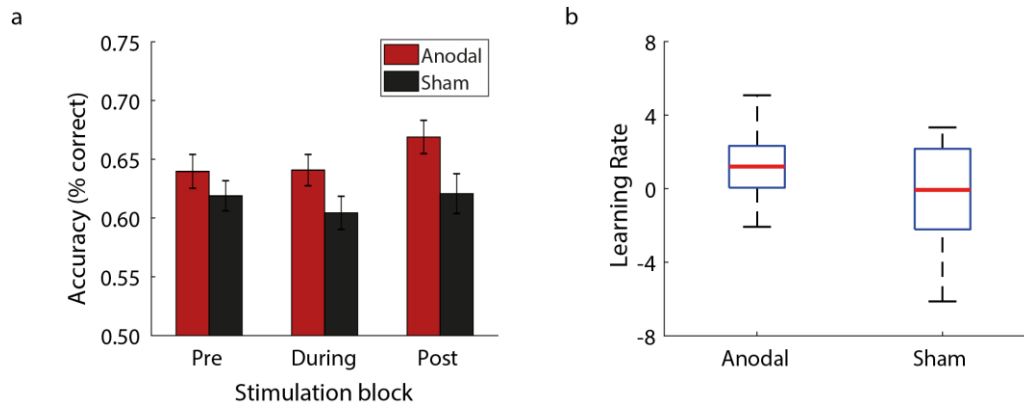
**Figure 2. Behavioural performance**: (a) Mean behavioural performance across participants per group (Anodal, Sham) and block (Pre, During, Post). Error bars indicate standard error of the mean across participants. (b) Boxplot of learning rate across training showing faster learning for Anodal than Sham group. The upper and lower error bars display the minimum and maximum data values, and the central box represents the interquartile range (25th–75th percentiles). The red line in the centre of the box represents the median.
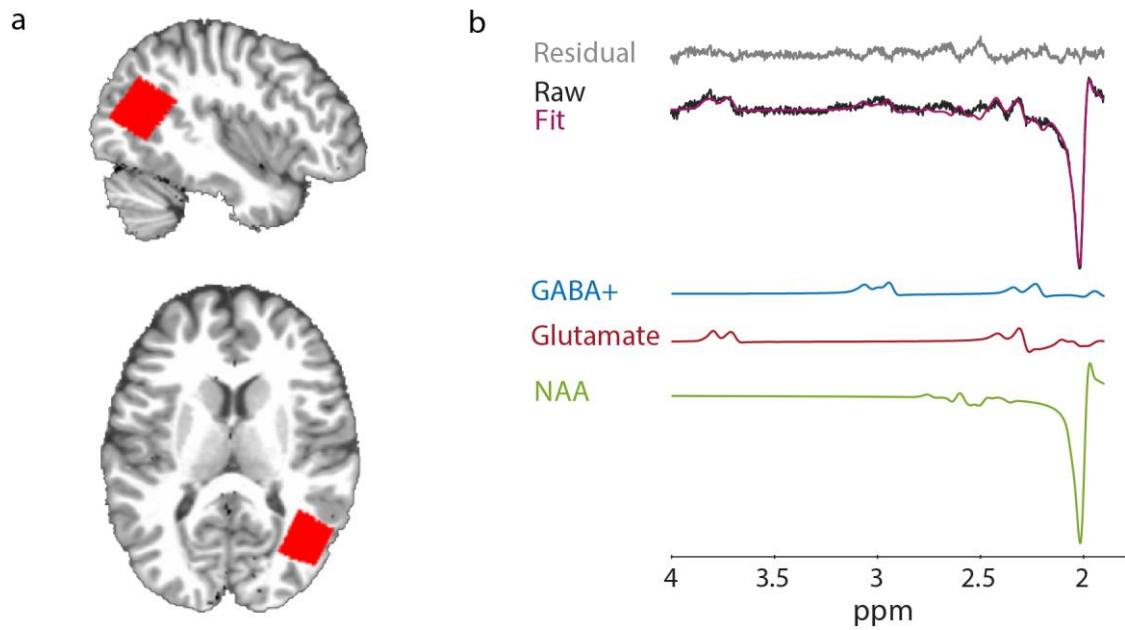
**Figure 3. MRS voxel placement and spectra**: (a) For each participant, we positioned the OCT MRS voxel using anatomical landmarks (superior temporal gyrus and middle occipital gyrus) on the acquired T1 scan to ensure that voxel placement was consistent across participants. Placement of the MRS voxel is shown for a representative participant (sagittal, axial view: native space). (b) Sample spectra from the MRS voxel of a representative participant. We show the LC model fit, the residual and the respective fits for GABA+, Glutamate and NAA.
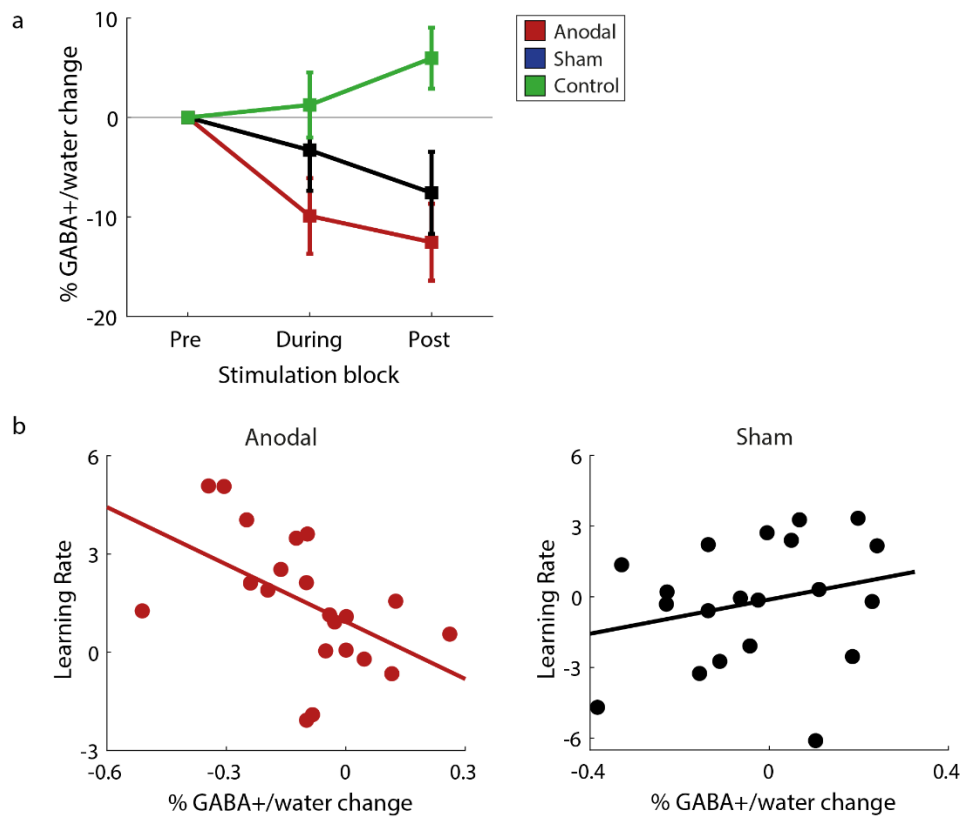
**Figure 4. GABA+ change during training and correlations with behaviour**: (a) OCT MRS-measured GABA+ over time is shown per group (Anodal, Sham, Control). We calculated % GABA+/water change by subtracting GABA+/water measurements in each of the three blocks from the pre-stimulation block and then divided by GABA+/water in the pre-stimulation block. (b) Skipped Pearson correlations showing a significant negative correlation of OCT GABA+ change (i.e. during- minus pre-stimulation block, divided by pre-stimulation block) with learning rate for the Anodal, but not the Sham group. These correlations were significantly different between groups.
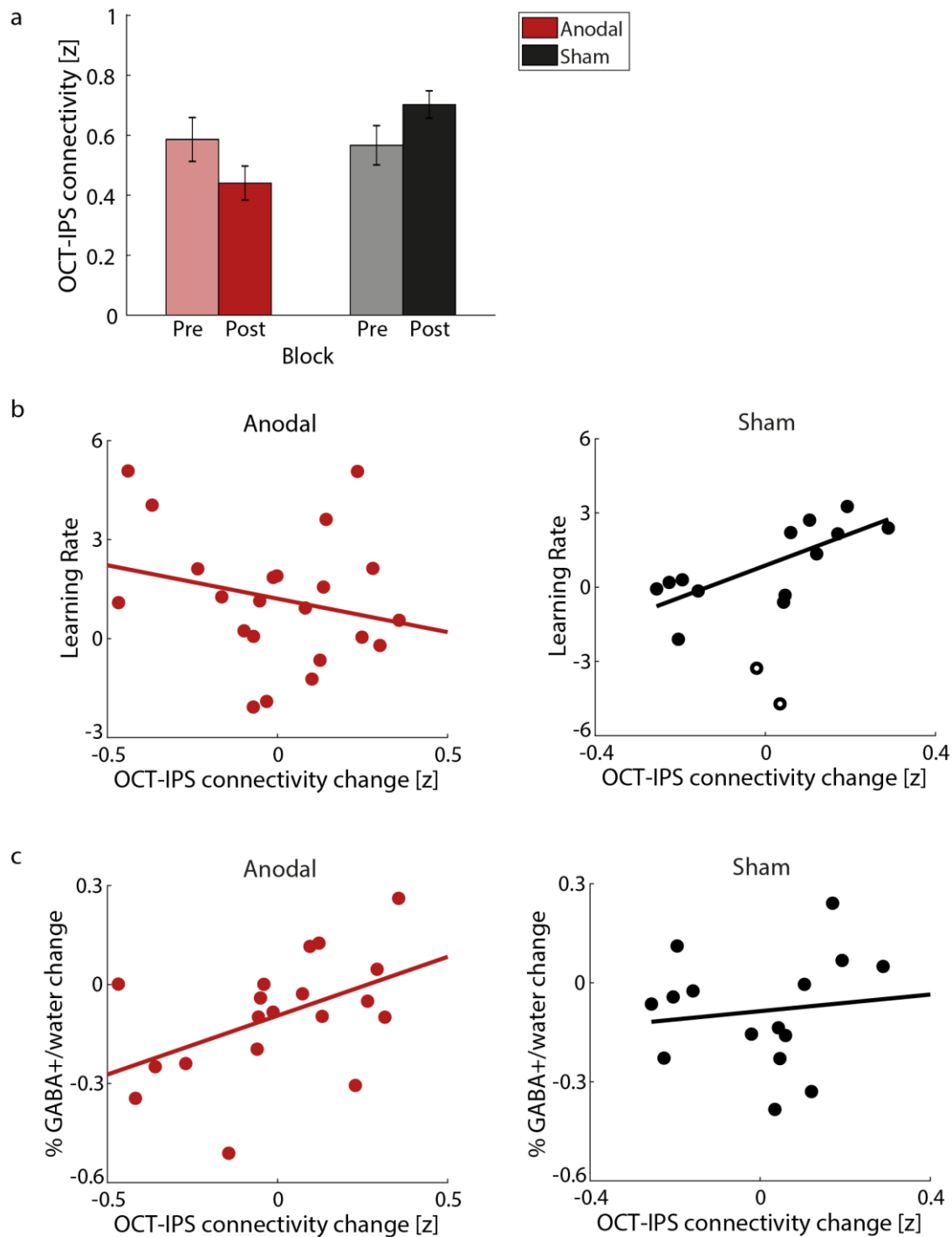
**Figure 5. Extrinsic connectivity and correlations with behaviour and GABA+:** (a) Mean OCT-IPS connectivity (Fisher z) per group (Anodal, Sham) and block (pre-, post-intervention). (b) Skipped Pearson correlations showing no significant correlation of OCT-IPS connectivity change with learning rate for the Anodal group, but a significant positive correlation for the Sham group. These correlations were significantly different between groups. (c) Skipped Pearson correlations showing a significant positive correlation of OCT-IPS connectivity change with OCT GABA+ change for the Anodal group, but not the Sham. Open symbols denote outliers.
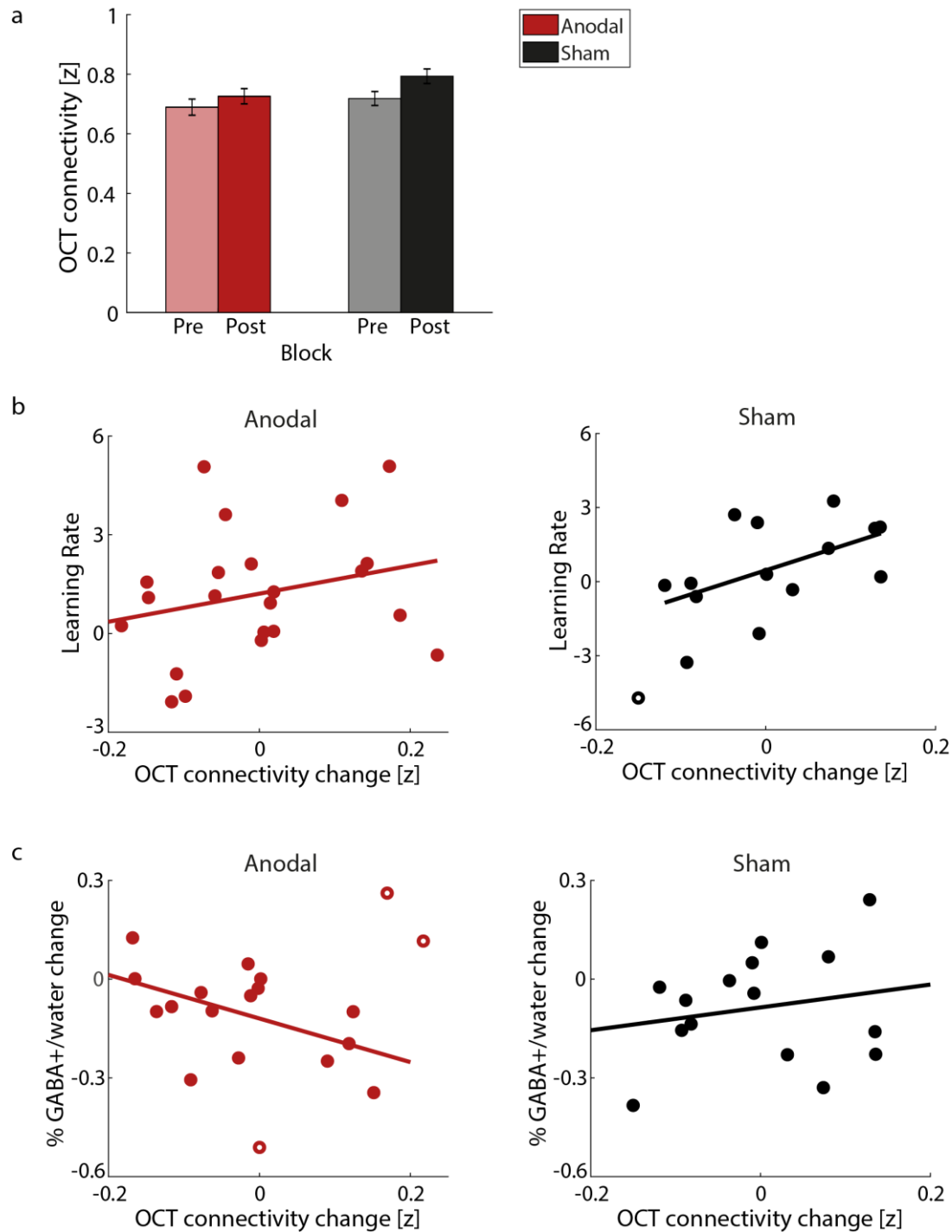
**Figure 6: Intrinsic connectivity and correlations with behaviour and GABA+:** (a) Mean intrinsic connectivity in OCT (Fisher z) per group (Anodal, Sham) and block (pre-, post-intervention). (b) Skipped Pearson correlations showing no significant correlation of OCT connectivity change with learning rate for the Anodal or the Sham group. (c) Skipped Pearson correlations showing a significant negative correlation of OCT connectivity change with OCT GABA+ change for the Anodal group, but not the Sham. Open symbols denote outliers.
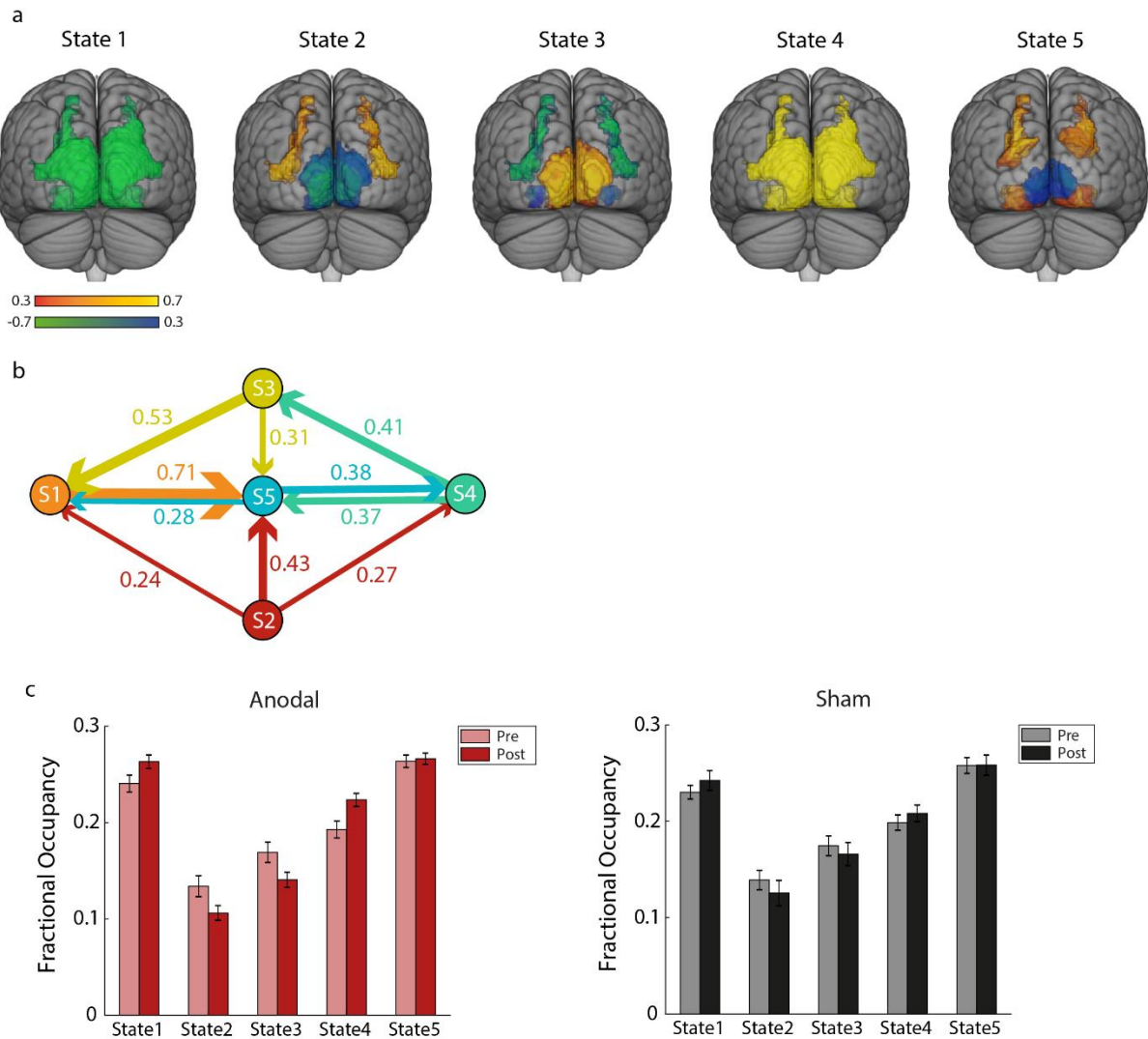
**Figure 7: HMM states and Fractional Occupancy change**: (a) Normalised mean activation maps per state are shown overlaid on the MNI brain. Warm colours (red-yellow) denote positive values, cool colours (blue-green) denote negative values for the respective region. (b) Transition probabilities between these states. The five states are displayed as nodes and the arrows denote the direction of the transition from one state to another. The thickness of the arrows is proportional to the transition probability between the corresponding states. Transition probabilities lower than 20% were removed for visualisation purposes. (c) Mean Fractional Occupancy per state and block (pre-, post-intervention) are shown for each group (Anodal: left, Sham: right). Lighter bars correspond to pre-training measures, darker bars to post-training measures.
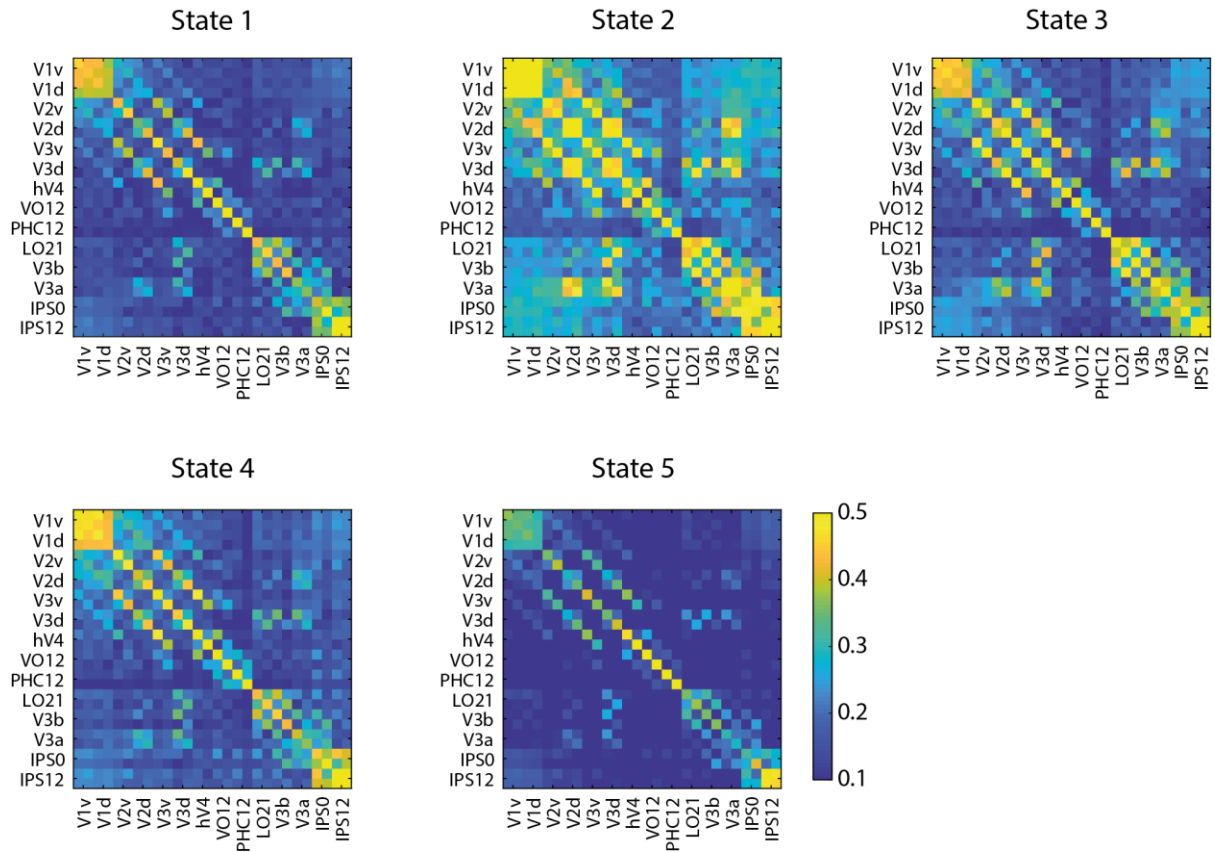
**Figure S1: Functional Connectivity matrices of HMM states**: Functional Connectivity matrices are shown as 28x28 matrices per state. For each ROI, data are included for each hemisphere (left, right). Warm colours (yellow) denote higher connectivity values, cool colours (blue) denote connectivity values close to zero.

## Supplementary Tables

**Table S1. MRS quality measures**: Cramer-Rao lower bound (CRLB), linewidth and signal-to-noise ratio (SNR) are shown for the OCT MRS voxel per group and block.

| MRS quality measure | Block | Group | Mean | Std |
|---|---|---|---|---|
| **CRLB** | Pre | Anodal | 5.67 | 1.20 |
| | | Sham | 5.65 | 1.14 |
| | | Control | 5.91 | 1.31 |
| | During | Anodal | 6.76 | 2.00 |
| | | Sham | 6.35 | 2.13 |
| | | Control | 6.23 | 1.27 |
| | Post | Anodal | 6.81 | 1.89 |
| | | Sham | 6.50 | 1.73 |
| | | Control | 5.82 | 1.05 |
| **Linewidth** | Pre | Anodal | 7.83 | 0.67 |
| | | Sham | 7.96 | 0.45 |
| | | Control | 8.14 | 0.48 |
| | During | Anodal | 7.94 | 0.70 |
| | | Sham | 8.07 | 0.50 |
| | | Control | 8.20 | 0.53 |
| | Post | Anodal | 7.95 | 0.68 |
| | | Sham | 8.15 | 0.49 |
| | | Control | 8.22 | 0.56 |
| **SNR** | Pre | Anodal | 19.95 | 3.40 |
| | | Sham | 20.50 | 2.98 |
| | | Control | 19.27 | 3.58 |
| | During | Anodal | 19.33 | 3.50 |
| | | Sham | 20.00 | 3.34 |
| | | Control | 18.68 | 3.63 |
| | Post | Anodal | 20.29 | 3.77 |
| | | Sham | 20.15 | 3.01 |
| | | Control | 18.91 | 3.44 |

**Table S2: Control analyses for GABA+ correlation with behaviour**: Pearson correlations (r, p) for GABA+ change and learning rate when: regressing out the CSF percentage or using α-correction to control for tissue composition within the MRS mask, using GABA+ referenced to NAA (rather than water), regressing out changes in MRS data quality (linewidth, SNR), and testing for neurotransmitter specificity (Glu change).

| Group | Control | r | p |
|-------|---------|------|-------|
| **Anodal** | %CSF | -0.52 | 0.017 |
| | α-correction | -0.51 | 0.018 |
| | GABA+/NAA | -0.47 | 0.031 |
| | Linewidth | -0.49 | 0.024 |
| | SNR | -0.50 | 0.022 |
| | Glu | -0.28 | 0.225 |
| **Sham** | %CSF | 0.25 | 0.291 |
| | α-correction | 0.26 | 0.262 |
| | GABA+/NAA | 0.27 | 0.248 |
| | Linewidth | 0.25 | 0.291 |
| | SNR | 0.27 | 0.251 |
| | Glu | -0.07 | 0.782 |

**Table S3: Control analyses for GABA+ correlation with resting-state connectivity**: Pearson correlations (r, p) for GABA+ change and resting-state connectivity when: regressing out the CSF percentage or using α-correction to control for tissue composition within the MRS mask, using GABA+ referenced to NAA (rather than water), regressing out changes in MRS data quality (linewidth, SNR), and testing for neurotransmitter specificity (Glu change).

| Connectivity | Group | Control | r | p |
|---|---|---|---|---|
| OCT-IPS | Anodal | %CSF | 0.48 | 0.039 |
| | | α-correction | 0.50 | 0.030 |
| | | GABA+/NAA | 0.51 | 0.025 |
| | | Linewidth | 0.49 | 0.032 |
| | | SNR | 0.48 | 0.037 |
| | | Glu | 0.03 | 0.909 |
| | Sham | %CSF | 0.24 | 0.396 |
| | | α-correction | 0.12 | 0.667 |
| | | GABA+/NAA | 0.19 | 0.495 |
| | | Linewidth | 0.14 | 0.620 |
| | | SNR | 0.13 | 0.656 |
| | | Glu | -0.22 | 0.426 |
| OCT | Anodal | %CSF | -0.50 | 0.048 |
| | | α-correction | -0.53 | 0.035 |
| | | GABA+/NAA | -0.54 | 0.033 |
| | | Linewidth | -0.52 | 0.037 |
| | | SNR | -0.51 | 0.045 |
| | | Glu | 0.08 | 0.773 |
| | Sham | %CSF | 0.29 | 0.299 |
| | | α-correction | 0.20 | 0.466 |
| | | GABA+/NAA | 0.25 | 0.377 |
| | | Linewidth | 0.26 | 0.358 |
| | | SNR | 0.26 | 0.353 |
| | | Glu | -0.13 | 0.633 |

**Table S4. Visual regions for time-varying connectivity analysis**: Regions were selected from the Probabilistic map of Visual Topography (Wang et al., 2015). The size and the MNI coordinates of the centre of gravity for each region are shown. Regions between 30 and 100 voxels were grouped together with a neighbouring region that serves similar functionality and displayed a similar time course. Regions smaller than 30 voxels were excluded from the analysis as signals being unreliable.

| Region | Hem. | Size | x | y | z |
|---|---|---|---|---|---|
| V1v | L | 462 | -6 | -89 | -5 |
| | R | 394 | 8 | -87 | -2 |
| V1d | L | 389 | -7 | -96 | 2 |
| | R | 359 | 11 | -94 | 5 |
| V2v | L | 359 | -9 | -83 | -11 |
| | R | 368 | 10 | -81 | -8 |
| V2d | L | 309 | -10 | -99 | 12 |
| | R | 336 | 15 | -96 | 14 |
| V3v | L | 247 | -17 | -79 | -12 |
| | R | 280 | 18 | -77 | -11 |
| V3d | L | 264 | -18 | -97 | 16 |
| | R | 253 | 24 | -94 | 16 |
| hV4 | L | 155 | -25 | -80 | -14 |
| | R | 173 | 26 | -79 | -12 |
| VO1, VO2 | L | 192 | -25 | -66 | -10 |
| | R | 214 | 26 | -64 | -9 |
| PHC1, PHC2 | L | 176 | -27 | -52 | -8 |
| | R | 164 | 28 | -49 | -9 |
| LO1, LO2 | L | 228 | -35 | -88 | 7 |
| | R | 221 | 38 | -85 | 9 |
| V3b | L | 111 | -29 | -90 | 17 |
| | R | 152 | 34 | -84 | 18 |
| V3a | L | 195 | -19 | -91 | 24 |
| | R | 359 | 21 | -88 | 28 |
| IPS0 | L | 264 | -25 | -80 | 30 |
| | R | 235 | 30 | -78 | 33 |
| IPS1, IPS2 | L | 206 | -21 | -71 | 46 |
| | R | 155 | 25 | -69 | 47 |

**Table S5: Control analyses for time-varying connectivity analysis**: Repeated measures ANOVA results (State x Block interaction on Fractional Occupancy) are shown per group for a range of HMM parameters (states: from 4 to 7, PCA: from 70% to 100% in increments of 10%). F and p-values are reported per test and the significant results are shown in italic.

| Model | Group | F | p |
|---|---|---|---|
| states=4, PCA=70% | *Anodal* | *7.36* | *0.006* |
| | Sham | 0.62 | 0.486 |
| states=4, PCA=80% | *Anodal* | *7.81* | *0.006* |
| | Sham | 1.12 | 0.318 |
| states=4, PCA=90% | *Anodal* | *7.42* | *0.009* |
| | Sham | 1.10 | 0.318 |
| states=4, PCA=100% | *Anodal* | *9.70* | *0.004* |
| | Sham | 1.73 | 0.210 |
| states=5, PCA=70% | *Anodal* | *5.55* | *0.013* |
| | Sham | 0.74 | 0.451 |
| states=5, PCA=80% | *Anodal* | *6.22* | *0.010* |
| | Sham | 1.14 | 0.319 |
| states=5, PCA=90% | *Anodal* | *7.50* | *0.007* |
| | Sham | 0.66 | 0.474 |
| states=5, PCA=100% | *Anodal* | *7.59* | *0.005* |
| | Sham | 1.84 | 0.194 |
| states=6, PCA=70% | *Anodal* | *5.99* | *0.005* |
| | Sham | 0.41 | 0.688 |
| states=6, PCA=80% | *Anodal* | *6.84* | *0.005* |
| | Sham | 0.52 | 0.598 |
| states=6, PCA=90% | *Anodal* | *7.23* | *0.008* |
| | Sham | 0.54 | 0.536 |
| states=6, PCA=100% | *Anodal* | *6.93* | *0.009* |
| | Sham | 1.87 | 0.190 |
| states=7, PCA=70% | *Anodal* | *4.38* | *0.013* |
| | Sham | 0.47 | 0.688 |
| states=7, PCA=80% | *Anodal* | *5.40* | *0.008* |
| | Sham | 0.65 | 0.556 |
| states=7, PCA=90% | *Anodal* | *6.52* | *0.008* |
| | Sham | 0.63 | 0.521 |
| states=7, PCA=100% | *Anodal* | *4.84* | *0.009* |
| | Sham | 1.54 | 0.237 |

**Table S6: Minimum Reporting Standards in MRS checklist**

| Site (Name or Number) | MRC Cognition and Brain Sciences Unit (University of Cambridge) |
|---|---|
| **1. Hardware** | |
| a. Field strength [T] | 3 |
| b. Manufacturer | Siemens |
| c. Model | Prisma |
| d. RF coils | 32-channel receive head coil |
| e. Additional hardware | N/A |
| **2. Acquisition** | |
| a. Pulse sequence | MEGA-PRESS |
| b. Volume of Interest (VOI) locations | Occipito-temporal cortex |
| c. Nominal VOI size [$cm^3$, $mm^3$] | 20x20x25 mm |
| d. Repetition Time (TR), Echo Time (TE) [ms, s] | TR=3000ms, TE=68ms |
| e. Total number of Excitations or acquisitions per spectrum | 256 |
| f. Additional sequence parameters: | Spectral bandwidth: 1200 Hz<br><br>Spectral points: 2048 |
| g. Water Suppression Method | Water suppression was achieved using variable power with optimized relaxation delays and outer volume suppression. |
| h. Shimming Method, reference peak, and thresholds for "acceptance of shim" chosen | Automated 3D head shim (GRE-BRAIN) to achieve water peak linewidth below 10 Hz. |
| i. Triggering or motion correction method | N/A |

| 3. Data analysis methods and outputs | |
|---|---|
| a. Analysis software | MRspa (preprocessing, version v1.5c), LCmodel (fitting and quantification) |
| b. Processing steps deviating from quoted reference or product | MRspa pre-processing options selected:<br><br>- eddy current corr.: ECC2 + zero phase<br><br>- frequency corr.: absolute (3.01)<br><br>- phase corr.: least square |
| c. Output measure | Concentrations relative to water or NAA |
| d. Quantification references and assumptions, fitting model assumptions | We fitted model spectra of γ-amino-butyric acid (GABA), Glutamate (Glu), Glutamine (Gln) and N acetylaspartate (NAA) to the edited spectra. The model spectra of were generated based on previously reported chemical shifts and coupling constants using the GAMMA/PyGAMMA simulation library of VESPA for carrying out the density matrix formalism. A 20 x 20 spatial matrix was used to simulate the spatial variations inside and outside the nominal PRESS dimensions. Simulations were performed with the same RF pulses and sequence timings as that on the 3T system in use. |
| 4. Data Quality | |
| a. Reported variables | See Table S1 |
| b. Data exclusion criteria | Water peak linewidth > 10 Hz<br><br>CRLB > 15%<br><br>GABA+ concentration outside three standard deviations from the mean across all groups and blocks. |
| c. Quality measures of postprocessing Model fitting | See Table S1 |
| d. Sample Spectrum | See Figure 3 |